MICROWAVE PROPAGATION IN N-TYPE GERMANIUM SUBJECTED TO A HIGH ELECTRIC FIELD

MICROWAVE PROPAGATION IN N-TYPE GERMANIUM SUBJECTED TO A HIGH ELECTRIC FIELD

By

MOHAMMAD HASIB UR RAHMAN, B. Sc. Eng., M. Sc. Eng.

A Thesis

Submitted to the Faculty of Graduate Studies

in Partial Fulfilment of the Requirements

for the Degree

Master of Engineering

McMaster University

April, 1967

MASTER OF ENGINEERING (1967)
(Electrical Engineering)

McMASTER UNIVERSITY
Hamilton, Ontario

TITLE: Microwave Propagation in n-type Germanium Subjected to a High Electric Field

AUTHOR: Mohammad Hasib ur Rahman B. Sc. (East Pakistan Engineering University, Dacca)
M. Sc. (East Pakistan Engineering University, Dacca)

SUPERVISOR: Professor M. W. Gunn

NUMBER OF PAGES: xii, 89

SCOPE AND CONTENTS:

Measurements of the propagation characteristics of 10 ohm-cm. n-type germanium subjected to a high electric field have been carried out at 9.522 GHz with a microwave reflection bridge. The experimental arrangement enabled measurements to be made with the microwave and applied electric field vectors both parallel and at right angles. The expressions for the co-efficient at a particular measuring plane in the reflection bridge are derived.

The absolute resistivity and dielectric constant obtained by microwave measurement are compared with those of d.c. measurement and found to be in close agreement.

Theoretical expressions for the performance of a hot electron microwave rotator are also developed.

ABSTRACT

A method for the measurement of the microwave conductivity of a semiconductor subjected to a high electric field is described, which provides for varying angles between the microwave and applied electric field vectors. The results of measurements on 10 ohm-cm. n-type germanium at 9.522 GHz with applied electric fields up to 3KV/cm. are given.

The measurements show that the microwave conductivity is controlled by the differential carrier mobility $(\frac{\partial \nu}{\partial E})$ for the condition of microwave and applied electric field vectors parallel. For the case of the fields at right angles the microwave conductivity is controlled by a carrier mobility intermediate between the d.c. mobility $(\frac{\nu}{E})$ and the differential mobility $(\frac{\partial \nu}{\partial E})$.

Theoretical expressions for the performance of a proposed "Hot Electron Microwave Rotator" are developed.

ACKNOWLEDGEMENTS

The author expresses his deep sense of gratitude to Dr. M. W. Gunn for his kind and constant guidance throughout the progress of the work.

The author also expresses his gratitude to the Government of Canada for the receipt of a Commonwealth Scholarship which made this investigation possible.

Thanks are also due to Miss Marlene Schultz for typing this manuscript in such a short time.

TABLE OF CONTENTS

LIST OF SYMBOLS

α = attenuation constant; angle between d.c. field and microwave field vectors.

α_x, α_y = attenuation constants due to x, y components of an electromagnetic wave in axial (z) direction.

a, b = waveguide dimensions; incident and reflected waves; semi-major and minor axes; constants.

A, B, C = constants in the expression for reflection co-efficient; A = twice the difference in the attenuator readings.

A_1, A_r = attenuator readings with sample terminated by a short.

A_o, $A_r(s_1)$ = attenuator readings with fixed short

β = phase constant.

β_r, β_o = phase constant in the empty wave guide.

β_x, β_y = phase constants due to x, y components of the wave in z direction

C_s = $\frac{|Z_n|}{\beta_o d}$

d = sample thickness.

d_1 = distance of the fixed short from measuring plane.

δ = skin depth; angle between the semi-major axis and x-axis.

e = magnitude of electronic charge.

ε = absolute permittivity of semi-conductor

ε_r = relative dielectric constant.

ε_o = absolute free space permittivity.

E = d.c. electric field

ΔE = change in d.c. electric field.

E_1, E_o = peak microwave field.

E_x = component of microwave field along x-axis.

E_y = component of microwave field along y-axis.

E_x' = component of microwave field along the major axis.

E_y' = component of microwave field along the minor axis.

$\mathcal{E}_L$ = thermal equilibrium energy of the carrier.

$\mathcal{E}_o$ = energy of the carrier at an electric field.

$\Delta\mathcal{E}$ = change in carrier energy due to microwave field.

f = frequency

f_o = frequency of optical phonon.

F = figure of merit.

GHz = giga hertz

Ge = germanium

h = Planck's constant.

H = magnetic field.

I = current

K = Boltzman's constant.

K_A = residual attenuation of the attenuator.

K_S = zero setting and fixed loss of the short circuit

ℓ = mean free path between collisians

ℓ_1, ℓ_r = precision short reading with the sample terminated by a short.

ℓ_o, $\ell(s_1)$ = precision short reading with the fixed short.

$\ell_r(Z_o)$ = precision short reading with a load Z_o.

ℓ_s = distance of the measuring plane from port 2.

L = length of the sample.

m = mass of an electron.

μ = mobility

μ_o = low field mobility; free space permeability.

$\mu_\perp$ = microwave mobility for the conditions of perpendicular microwave and applied electric vectors.

n = number of electrons/unit volume.

n_1, n_2 = constants.

P = average power carried by the wave.

ψ = angle of rotation or angular shift.

ϕ = twice the difference in precision short readings with the sample terminated by a short and with the fixed short.

ρ = reflection co-efficient; resistivity.

$\rho(o)$ = reflection co-efficient of the air-sample interface.

$\rho(x)$ = reflection co-efficient at a measuring plane.

$\rho(\varepsilon_1)$ = reflection co-efficient at the fixed short.

σ = semiconductor conductivity.

$d\sigma$ = differential conductivity.

$\sigma_{d.c.}$ = d.c. conductivity.

$\hat{\sigma}$ = complex conductivity.

σ' = apparent conductivity.

$\sigma_{\parallel}$ = microwave conductivity for conditions of parallel microwave and electric field vectors.

$\sigma_\perp$ = microwave conductivity for conditions of perpendicular microwave and applied electric field vectors.

R = resistance

R_e = equivalent resistance

R_o = low field resistance of the sample.

S = scattering matrix

t = time.

τ = angle in von Hippel graphs; relaxation time.

τ_m = momentum relaxation time.

τ_ε = energy relaxation time.

$\tau_{\varepsilon o}$ = energy relaxation time corresponding to E

τ_o = optical phonon relaxation time.

T = thermal equilibrium temperature of an electron; magnitude in von Hippel graphs.

T_e = temperature of an electron at an electric field.

θ = angle between d.c. field and microwave field.

u = velocity of acoustic phonons.

v, v_d = drift velocity of an electron.

v_s = saturation drift velocity of an electron.

v_T = thermal velocity for an electron energy KT.

$\frac{v}{E}$ = d.c. mobility.

$\frac{\partial v}{\partial E}$ = differential mobility.

V = voltage.

ω = radian frequency.

x, y, z = cartesian co-ordinates

x', y' = new position of the axis of the ellipse.

z = distance in the direction of propagation.

Z_1 = impedance of the empty wave guide.

$Z(o)$ = input impedance of the air-sample interface.

Z_x = wave impedance due to the x-component of the wave in z-direction.

γ = propagation constant.

γ_1, γ_2 = propagation constant of empty and semi-conductor filled wave guide respectively.

γ_s = propagation constant of the sample arm.

λ_1, λ_g = wavelength in empty and semi-conductor filled wave guides respectively.

§ = angle of C_s.

$\parallel$ = conditions of parallel microwave and applied electric field vectors.

$\perp$ = conditions of perpendicular microwave and applied electric field vectors.

CHAPTER I

INTRODUCTION

This thesis describes a method of measurement of the microwave conductivity of a semiconductor subjected to a high electric field, which allows the angle between the microwave and applied d.c. electric field vectors to be varied. The method depends on the use of microwave reflection bridge and gives a means of measurement of the propagation constant of a wave propagating in the semiconductor.

The theory of operation of this measuring system is developed and the results of measurements on 10 ohm-cm. n-type germanium are given. A possible application of the propagation phenomena described is a "Hot Electron Rotator" and theoretical work on the performance of such a device is presented.

1.1 HOT CARRIERS:

When an electric field is applied to a semiconductor, the carriers are accelerated gaining energy and momentum from the field. This excess energy and momentum are dissipated by the interaction of phonons (acoustic and optical) with the carriers. The rates of energy and momentum loss by the carriers are described by the energy and momentum relaxation times τ_ε and τ_m.

At high fields, the carriers absorb so much energy from the field that the temperature of the carriers becomes significantly higher than that of the lattice. The carriers are then designated as "warm" or "hot" carriers according to the magnitude of the kinetic energy resulting from the applied field. The idea of hot carriers was first introduced by Fröhlich[1] in 1947 in connection with the theory of dielectric breakdown. Figure 1 shows the variation of energy and temperature with electric field. As the carrier energy increases, the momentum relaxation time τ_m decreases and hence the carrier mobility decreases. This leads to the saturation of drift velocity at high electric fields. This decrease in carrier mobility and resultant deviation from Ohm's law in Ge at high fields have been studied by Ryder and Shockley[2-4], Gunn[5] and Larrabee[6], who obtained the saturation drift velocity v_s in the range 4.5-9 KV/cm. The most recent measurements have been reported in a number of papers written by workers at Stanford University and California Institute of Technology.[7]

1.2 LITERATURE SURVEY:

The behaviour of semiconductors in microwave and pulsed fields has been investigated by a number of authors[8-15].

Arthur et al[10] showed that microwave attenuations in presence of high field is proportional to differential mobility $(\frac{\partial v}{\partial E})$ and that it decreases with increasing external electric field. He obtained saturation velocity v_s at 4.5 KV/cm. with 5 ohm-cm. germanium sample, in agreement with Ryder, Shockley and others.

Gibson et al[12] measured the propagation constant in Ge at

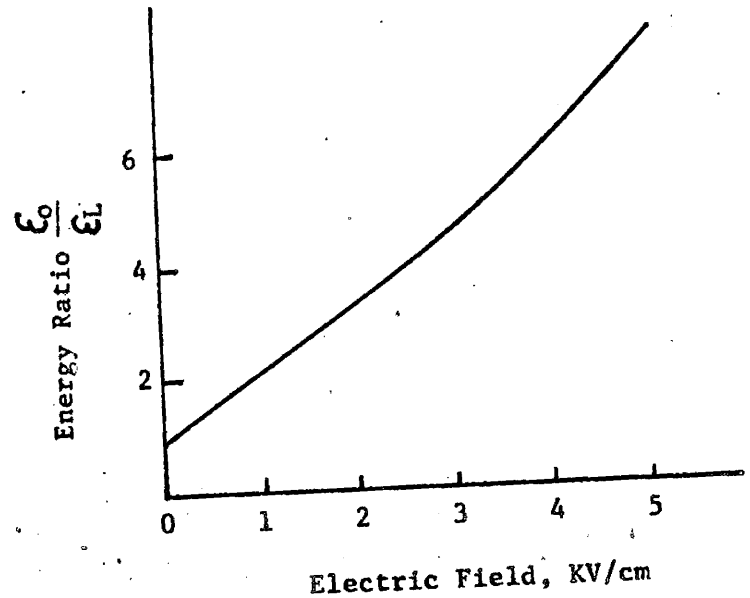

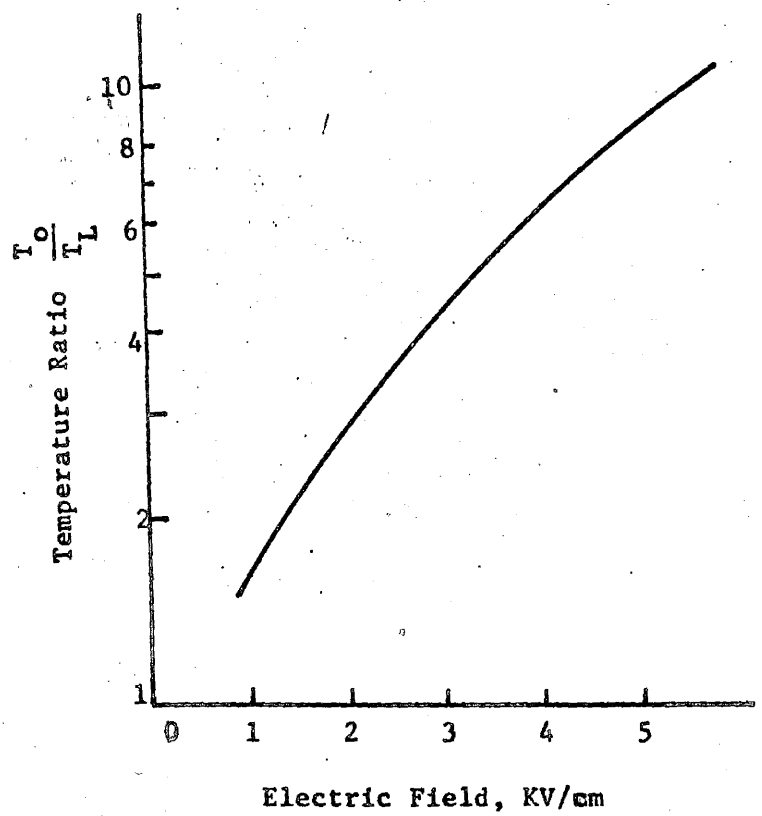

FIGURE 1: Variation of carrier energy ($\mathcal{E}_o$) and temperature (T_o) with electric field, compared with $\mathcal{E}_L$ and T_L, the thermal equilibrium values after Gibson etal[12].

34.75 GHz and showed that the microwave conductivity cannot be identified with the d.c. or differential mobility but it lies intermediate between d.c. and differential mobility.

Nag and Das[13] derived the microwave conductivity and change in apparent dielectric constant from the distribution function of the carriers in a semiconductor subjected to a small microwave field and a high d.c. field, considering only acoustic and optical phonon scatterings. However, their theoretical results do not agree with the experimental results of Gibson[12] in the acoustic phonon scattering region below 5KV/cm.

Gunn[14] showed that the parallel microwave conductivity $\sigma_{\parallel}$ of 10 ohm-cm. n-Ge at 9.392 GHz is governed by the differential mobility, and that the free carrier contribution to the dielectric constant is positive for applied fields above 500 V/cm.

A recent paper on this subject appeared in 1965 by Dykman[15] who performed a theoretical calculation of microwave conductivity under low d.c. field in the range 0-500V/cm., considering the impurity, intervalley and inter-electronic scattering.

1.3 ANISOTROPIC CONDUCTIVITY IN GERMANIUM AT HIGH ELECTRIC FIELD

It has been argued from physical reasoning by Gunn[16, 14] that in Ge, $\sigma_{\parallel}$ is governed by differential mobility $\frac{\partial v}{\partial E}$ and $\sigma_{\perp}$ is governed by d.c. mobility $\frac{v}{E}$.

Since differential mobility and d.c. mobility are different, $\sigma_{\parallel}$ and $\sigma_{\perp}$ are also different and hence the microwave conductivity depends on the angle between the microwave field vector and d.c. electric field vector. A possible application of this effect is in the "Hot Electron Microwave Rotator" discussed in Chapter VII.

However, since at higher frequency[12] ($\omega\tau_{\varepsilon} >> 1$) $\sigma_{\parallel}$ approaches $\sigma_{\perp}$, it is clear that this proposed application of anisotropic conductivity at high electric field is limited to low frequency ($f \leq$ 10 GHz) and for a limited value of τ_{ε}.

The decrease of microwave attenuation in Ge at high electric field offers the prospect of very fast modulators and switches which would operate in the nano-second region.

CHAPTER II

THEORETICAL CONSIDERATIONS

2.1 DEPENDENCE OF CONDUCTIVITY AND DIELECTRIC CONSTANT ON THE FREQUENCY AND THE CARRIER ENERGY

The mobility of a semiconductor subjected to a high field of radian frequency ω at thermal equilibrium is given by[12]

$$\mu = \frac{e}{m} \left\langle \frac{\tau_m}{1+j\omega\tau_m} \right\rangle \tag{2.1}$$

where the average value of momentum relaxation time

$$\langle \tau_m \rangle = \frac{\int_0^\infty \tau_m(\mathcal{E})\, \mathcal{E}^{\frac{3}{2}} e^{-\frac{\mathcal{E}}{KT}}\, d\mathcal{E}}{\int_0^\infty \mathcal{E}^{\frac{3}{2}} e^{-\frac{\mathcal{E}}{KT}} d\mathcal{E}} \tag{2.2}$$

and the complex conductivity

$$\hat{\sigma}(\omega) = \frac{ne^2}{m} \left\langle \frac{\tau_m}{1+j\omega\tau_m} \right\rangle$$

$$= \frac{ne^2}{m} \left\langle \frac{\tau_m}{1+\omega^2\tau_m^2} \right\rangle - j\omega \frac{ne^2}{m} \left\langle \frac{\tau_m^2}{1+\omega^2\tau_m^2} \right\rangle \tag{2.3}$$

where e, m are charge and mass of an electron respectively.

Maxwell's curl equation can be written as

$$\nabla \times H = (\hat{\sigma} + j\omega\epsilon)E$$

$$= \left[\frac{ne^2}{m} \left\langle \frac{\tau_m}{1+\omega^2\tau_m^2} \right\rangle + j\omega\left(\epsilon - \frac{ne^2}{m} \left\langle \frac{\tau_m^2}{1+\omega^2\tau_m^2} \right\rangle\right) \right] E \tag{2.4}$$

Equation 2.4 gives the conductivity,

$$\sigma' = \frac{ne^2}{m} \left\langle \frac{\tau_m}{1+\omega^2\tau_m^2} \right\rangle$$

$$= \frac{ne^2}{m} \langle \tau_m \rangle \qquad \text{[since at high fields } (\omega\tau_m)^2 \ll 1\text{]}$$

$$= \sigma_0 \tag{2.5}$$

and apparent dielectric constant,

$$\varepsilon_r' = \varepsilon_r - \frac{ne^2}{m\varepsilon_o} \left\langle \frac{\tau_m^2}{1+\omega^2\tau_m^2} \right\rangle$$

$$= \varepsilon_r - \frac{\sigma_o}{\varepsilon_o} \tau_m \tag{2.6}$$

The second term in equation (2.6) is the electronic contribution to dielectric constant.

When the semiconductor is subjected to a high electric field, equations (2.5) and (2.6) are changed to

$$\sigma' = \sigma_o \left[1 - 2n_1 \frac{\mathcal{E}_o - \mathcal{E}_L}{\mathcal{E}_o} \frac{T}{\tau_{\varepsilon_o}} \frac{1}{1+\omega^2T^2}\right] \tag{2.7}$$

$$\varepsilon_r' = \varepsilon_r - \frac{\sigma_o}{\varepsilon_o} \left[\tau_m - 2n_1 \frac{\mathcal{E}_o - \mathcal{E}_L}{\mathcal{E}_o} \frac{T^2}{\tau_{\varepsilon_o}} \frac{1}{1+\omega^2T^2}\right] \tag{2.8}$$

and

$$T = \frac{\tau_{\varepsilon_o}}{1 + (n_2+n_1) \frac{\mathcal{E}_o - \mathcal{E}_L}{\mathcal{E}_o}} \tag{2.9}$$

where $\mathcal{E}_L$ = thermal equilibrium energy of the carrier,

$\mathcal{E}_o$ = energy of the carrier at an electric field E,

n_1, n_2 = constants

$$\text{Also, } \tau_m = a\mathcal{E}^{-n_1} = a\,[\mathcal{E}_o + \Delta\mathcal{E}]^{-n_1}$$
$$\simeq a\mathcal{E}_o^{-n_1}\left[1 - n_1\frac{\Delta\mathcal{E}}{\mathcal{E}_o}\right] = \tau_{m_o}\left[1 - n_1\frac{\Delta\mathcal{E}}{\mathcal{E}_o}\right] \tag{2.10}$$

and similarly

$$\tau_\varepsilon = b\mathcal{E}^{-n_2} = \tau_{\varepsilon_o}\left[1 - n_2\frac{\Delta\mathcal{E}}{\mathcal{E}_o}\right] \tag{2.11}$$

where a, b are constants and $\Delta\mathcal{E}$ = change of carrier energy by microwave field.

In the absence of an electric field, $\mathcal{E}_o = \mathcal{E}_L$, so that equations (2.7) and (2.8) reduce to those of equations (2.5) and (2.6) and $T = \tau_{\varepsilon_o}$, confirming the validity of these equations.

(a) EFFECT OF HIGH FREQUENCIES

At high frequencies $(\omega T)^2$ approaches infinity and the second terms in the parenthesis of equations (2.7) and (2.8) vanish, resulting

$$\sigma' = \sigma_o$$

and

$$\varepsilon_r' = \varepsilon_r - \frac{\sigma_o \tau_m}{\varepsilon_o}$$

(b) EFFECT OF LOW FREQUENCIES

At low frequencies $(\omega T)^2 << 1$, so that the equations (2.7) and (2.8) reduce to

$$\sigma' = \sigma_o \left[1 - 2n_1 \frac{\mathcal{E}_o - \mathcal{E}_L}{\mathcal{E}_o} \frac{1}{1 + (n_2+n_1)\frac{\mathcal{E}_o - \mathcal{E}_L}{\mathcal{E}_o}}\right]$$

$$\approx ne\,\mu_o \left[1 - 2n_1 \frac{\mathcal{E}_o - \mathcal{E}_L}{\mathcal{E}_o}\right]$$

assuming $(n_2+n_1)\ \frac{\mathcal{E}_o - \mathcal{E}_L}{\mathcal{E}_o} << 1.$

Thus, the mobility is reduced at high carrier energy and

$$\varepsilon_r' = \varepsilon_r - \frac{\sigma_o}{\varepsilon_o}\left[\tau_m - 2n_1 \frac{\mathcal{E}_o - \mathcal{E}_L}{\mathcal{E}_o} \frac{\tau_{\varepsilon_o}}{\{1 + (n_2+n_1)\frac{\mathcal{E}_o - \mathcal{E}_L}{\mathcal{E}_o}\}^2}\right]$$

$$\approx \varepsilon_r - \frac{\sigma_o \tau_m}{\varepsilon_o} + \frac{2n_1\sigma_o}{\varepsilon_o}\frac{\mathcal{E}_o - \mathcal{E}_L}{\mathcal{E}_o} \frac{\tau_{\varepsilon_o}}{1 + 2(n_2+n_1)\frac{\mathcal{E}_o - \mathcal{E}_L}{\mathcal{E}_o}}$$

where the third term shows the positive contribution to dielectric constant at high electric field.

2.2 HOT ELECTRON THEORY

At low electric fields, the conductivity tensor is independent of the electric field, that is the electric current is ohmic, varying linearly with E. At high fields this linear relationship between current and electric field fails. Shockley[17] has pointed out that this deviation is more easily produced in semiconductors than in metals. Since the mean energy in a metal is 5 - 10 ev. and that in a semiconductor is $\frac{3KT}{2} \approx 0.039$ ev., a change in the mean energy of the order of KT is a large change in semiconductors, while it is a small change in case of metal.

(a) LOW FIELD CONDUCTION

The exact value of mobility for a Maxwellian velocity distribution is expressed[18] as

$$\mu = \frac{4}{3}\frac{e\,\ell}{m}\quad\frac{1}{\sqrt{\pi}\,v_T} \tag{2.12}$$

where $v_T = \sqrt{\frac{2KT}{m}}$, thermal velocity for an electron energy KT ,

m, e = mass and charge of an electron ,

ℓ = mean free path between collision.

The mobility is, therefore, independent of E but dependson the type of scattering processes, namely impurity and lattice scattering. The former dominates over the latter at low temperature while opposite is true for high temperature.

(b) CONDUCTION AT LOW, INTERMEDIATE AND HIGH ELECTRIC FIELDS

In this range E = 1 - 10KV/cm., electrons and long wavelength acoustic phonons interact.

The average rate of energy exchange due to acoustic phonons is given by[18]

$$\left\langle \frac{d\mathcal{E}}{dt} \right\rangle_{\text{phonons}} = \frac{8\,mu^2}{\ell\sqrt{\pi}}\sqrt{\frac{2KT_e}{m}}\left[1 - \frac{T_e}{T}\right]$$

where u = velocity of acoustic phonons,

ℓ = mean free path between collisions,

T_e = temperature of electron at an electric field E,

T = thermal equilibrium temperature of an electron.

At thermal equilibrium $T = T_e$ and hence $\left\langle \frac{d\mathcal{E}}{dt} \right\rangle_{phonon} = 0$ i.e. there is no average energy gain by the electrons due to collision.

Also, $\left\langle \frac{d\mathcal{E}}{dt} \right\rangle_{field} = e E v_d$

For steady state,

$$e E v_d + \frac{8mu^2}{\ell\sqrt{\pi}} \sqrt{\frac{2KT_e}{m}} \left[1 - \frac{T_e}{T}\right] = 0 \qquad (2.13)$$

Noting that, $v_d = \frac{\mu_h}{\mu_o} \mu_o E$, where μ_h = high field mobility

μ_o = low field mobility

$$= \frac{e \ell \left[\frac{8}{9\pi m K T_e}\right]^{1/2}}{e \ell \left[\frac{8}{9\pi m K T}\right]^{1/2}} \mu_o E$$

$$= \sqrt{\frac{T}{T_e}}\, \mu_o E \qquad (2.14)$$

and

$$\frac{8mu^2}{\ell\sqrt{\pi}} \left[\frac{2KT_e}{m}\right]^{1/2}$$

$$= \frac{32\, u^2 e}{\pi \times 3\, e\, \ell} \left[\frac{T_e}{T} \cdot \frac{9\pi K T_e m}{8}\right]^{1/2}$$

$$= \frac{32\, u^2 e}{3\pi} \sqrt{\frac{T_e}{T}}\, \frac{1}{\mu_o}, \text{ equation (2.13) reduces to}$$

$$e E^2 \sqrt{\frac{T}{T_e}}\, \mu_o + \frac{32\, u^2 e}{3\pi} \sqrt{\frac{T_e}{T}}\, \frac{1}{\mu_o} \left(1 - \frac{T_e}{T}\right) = 0$$

or $$\left(\frac{T_e}{T}\right)^2 - \left(\frac{T_e}{T}\right) - \frac{3\pi}{32} \left(\frac{\mu_o E}{u}\right)^2 = 0$$

or $$\frac{T_e}{T} = \frac{1 + \left[1 + 4 \cdot \frac{3\pi}{32} \left(\frac{\mu_o E}{u}\right)^2\right]^{1/2}}{2} \qquad (2.15)$$

considering positive sign only, since $\frac{T_e}{T}$ >1 at high field.

(i) Conduction at Low Fields

At E>1KV/cm., $\mu_o E \ll u$, so that

$$\frac{T_e}{T} = \frac{1 + [1 + \frac{1}{2} \frac{4 \times 3\pi}{32} (\frac{\mu_o E}{u})^2]}{2}$$ neglecting smaller terms or

$$\sqrt{\frac{T_e}{T}} = 1 - \frac{1}{2} \frac{3\pi}{32} (\frac{\mu_o E}{u})^2$$

By equation (2.14)

$$v_d = \mu_o [1 - \frac{1}{2} \frac{3\pi}{32} (\frac{\mu_o E}{u})^2] E \qquad (2.16)$$

which shows the decrease of mobility with E.

(ii) Conduction at Medium Fields

If the field is increased until $\mu_o E = \frac{8}{3} u$, the equation (2.15) reduces to

$$\frac{T_e}{T} = \frac{1 + \sqrt{(1 + \frac{8\pi}{3})}}{2}$$

$$\approx 2$$

and drift velocity drops to

$$v_d = \mu_o \sqrt{\frac{T}{T_e}} E$$

$$= 0.707 \mu_o E$$

(iii) Conduction at High Fields

At high field (E>10KV/cm.), $\mu_o E >> u$, so that equation (2.15) becomes

$$\frac{T_e}{T} \approx (\frac{3\pi}{32})^{\frac{1}{2}} \frac{\mu_o E}{u}$$

and by equation (2.14)

$$v_d = \mu_o \left[\frac{u}{\mu_o E} (\frac{32}{3\pi})^{1/2}\right]^{1/2} \} E$$

$$= [\mu_o \{ \frac{u}{\mu_o} (\frac{32}{3\pi})^{1/2} \}^{1/2}] E^{\frac{1}{2}}$$

where v_d is proportional to $\sqrt{E}$

and μ is proportional to $\frac{1}{\sqrt{E}}$

(c) CONDUCTION AT EXTREMLY HIGH FIELDS

At fields E> 60 KV/cm., electrons and optical phonons interact. When the value of v_d is such that $\frac{1}{2} m v_d^2$ is greater than optical phonon energy (hf_o), they will be excited directly from valence to conduction band.

If τ_o = relaxation time for optical modes, then[19]

$$(\frac{d\mathcal{E}}{dt})_{\text{phonons}} = - \frac{hf_o}{\tau_o}$$

Also,

$$(\frac{d\mathcal{E}}{dt})_{\text{Field}} = e E v_d$$

$$= e^2 \frac{\tau_o}{m} E^2$$

In a steady state,

$$\frac{hf_o}{\tau_o} = \frac{e^2 \tau_o}{m} E^2$$

or $$\tau_o = \frac{(hf_o m)^{1/2}}{e E}$$

and $$v_d = \frac{e}{m} \frac{(hf_o m)^{1/2}}{e E} E$$

$$= \left(\frac{hf_o}{m}\right)^{1/2} \qquad (2.17)$$

a constant showing saturation of drift velocity.

Using the energy of optical phonon, which is also known as the Raman energy (hf_o = .037 evfor Ge) and determined by neutron diffraction method,

$$v_d = 8 \times 10^6 \text{ cm./sec.}$$

This effect has been observed experimentally by Gunn[5] and is shown in Fig. 2.

At a voltage greater than 60KV/cm., the drift velocity increases suddenly, due to sudden increase in the current density by avalanche or ionisation.

2.3 D.C., DIFFERENTIAL AND MICROWAVE CONDUCTIVITY

The d.c. mobility (or the ease of movement of carriers) may be defined as the drift velocity per unit electric field i.e. $\mu = \frac{v}{E}$ and hence the d.c. conductivity,

$$\sigma_{d.c.} = ne \frac{v}{E} \qquad (2.18)$$

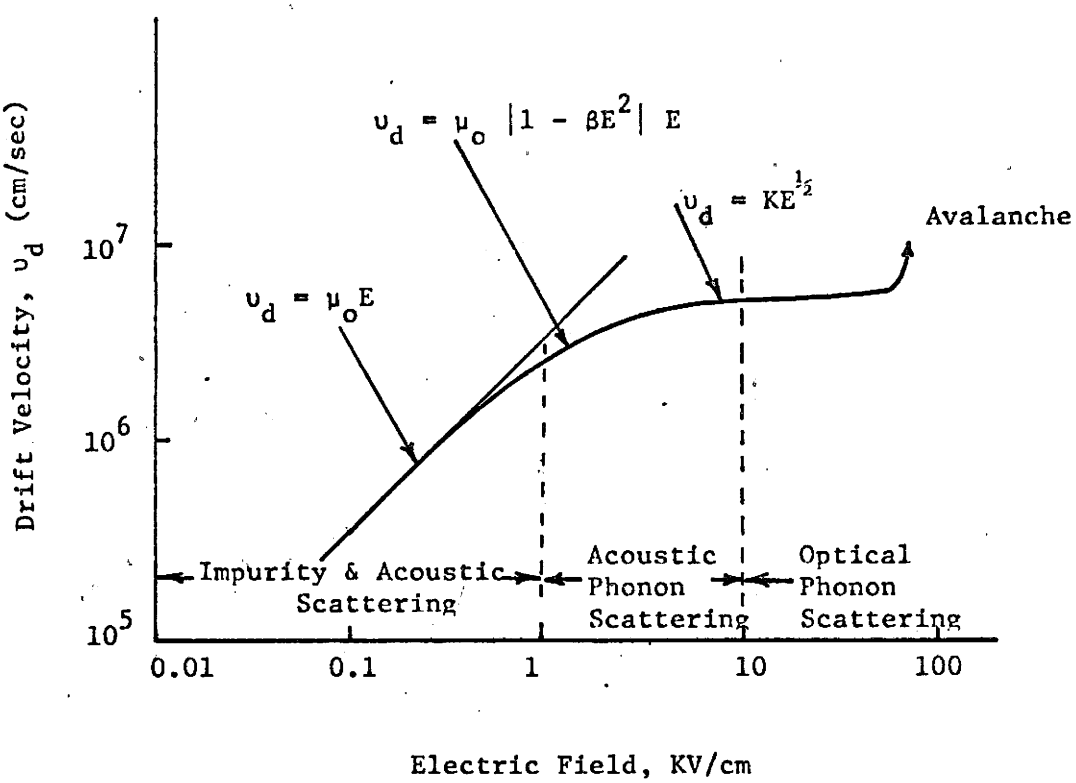

FIGURE 2: The variation of electron drift velocity with electric field for Ge (Gunn[5]).

The differential mobility is defined as the differential change of mobility with electric field i.e. $d\mu = \frac{\partial v}{\partial E}$ and hence the differential conductivity,

$$d\sigma = ne \frac{\partial v}{\partial E} \tag{2.19}$$

MICROWAVE CONDUCTIVITY

If the d.c. field E and peak microwave field E_1 are applied at an angle α (see fig. 3) with the assumption $E_1 << E$, then total field at plane z = 0,

$$E_t = E + \frac{E_1}{\sqrt{2}} (\cos \alpha + j \sin \alpha)$$

$$\therefore |E_t| = [(E + \frac{E_1}{\sqrt{2}} \cos \alpha)^2 + \frac{E_1^2}{2} \sin^2 \alpha]^{1/2}$$

$$= [E^2 + \frac{E_1^2}{2} + \sqrt{2}\, E\, E_1 \cos \alpha]^{1/2}$$

$$= E [1 + (\frac{E_1}{2E})^2 + \sqrt{2} \frac{E_1}{E} \cos \alpha]^{1/2}$$

$$\simeq E [1 + \frac{E_1}{\sqrt{2}\, E} \cos \alpha], \text{ neglecting } (\frac{E_1}{E})^2 \text{ as it is small.}$$

Hence the change in electric field in x direction,

$$\Delta E = |E_t| - E$$

$$= \frac{E_1}{\sqrt{2}} \cos \alpha \tag{2.20}$$

(i) Microwave Conductivity for Fields at Right Angles

Since, for $\alpha = 90°$, the change in electric field is zero, thereby resembling the case for no applied microwave field i.e.

$\mu_{\perp} = \frac{v}{E}$ and hence the perpendicular microwave conductivity,

$$\sigma_{\perp} = ne \frac{v}{E} \tag{2.21}$$

(ii) Microwave Conductivity for Parallel Fields

Since, for $\alpha = 0°$, the change in electric field is maximum (and so is the drift velocity change), i.e.

$$\mu_{\parallel} = \frac{\partial v}{\partial E}$$

and hence the parallel microwave conductivity,

$$\sigma_{\parallel} = ne \frac{\partial v}{\partial E} \tag{2.22}$$

Comparing equations (2.18) with (2.21) and (2.19) with (2.22),

$$\left.\begin{aligned} \sigma_{\perp} &= \sigma_{d.c.} \\ \text{and} \quad \sigma_{\parallel} &= d\sigma \end{aligned}\right\} \tag{2.23}$$

CHAPTER III

THEORY OF MEASUREMENT

3.1 PROPAGATION CONSTANT IN A SEMICONDUCTOR LOADED WAVE GUIDE

In a rectangular wave guide with dimensions a and b, a>b, the propagation constant γ_1 of the empty wave guide and γ_2 of the guide filled with semiconductor (see Fig. 4) are given by[20],

$$\gamma_1^2 = (j\beta_o)^2 = (\frac{\pi}{a})^2 - \omega^2\mu_o\varepsilon_o \tag{3.1}$$

and

$$\gamma_2^2 = (\alpha+j\beta)^2 = (\frac{\pi}{a})^2 - \omega^2\mu_o\varepsilon_o\,[\varepsilon_r - j\,\frac{\sigma}{\omega\varepsilon_o}] \tag{3.2}$$

where ω = radian frequency/second

σ = conductivity of the semiconductor

ε_o, μ_o = free space permittivity and permeability respectively.

Equating imaginary and real parts of equations (3.1) and (3.2) respectively, one can obtain:

$$\sigma = \frac{2\alpha\beta}{\omega\mu_o} \tag{3.3}$$

$$\varepsilon_r - 1 = \frac{\beta^2-\beta_o-\alpha^2}{\omega^2\mu_o\varepsilon_o} \tag{3.4}$$

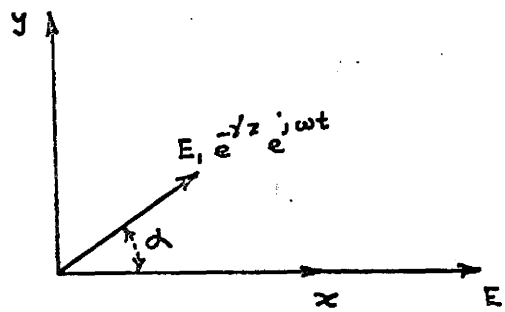

FIGURE 3: Relative positions of microwave and applied electric field vectors in a wave guide.

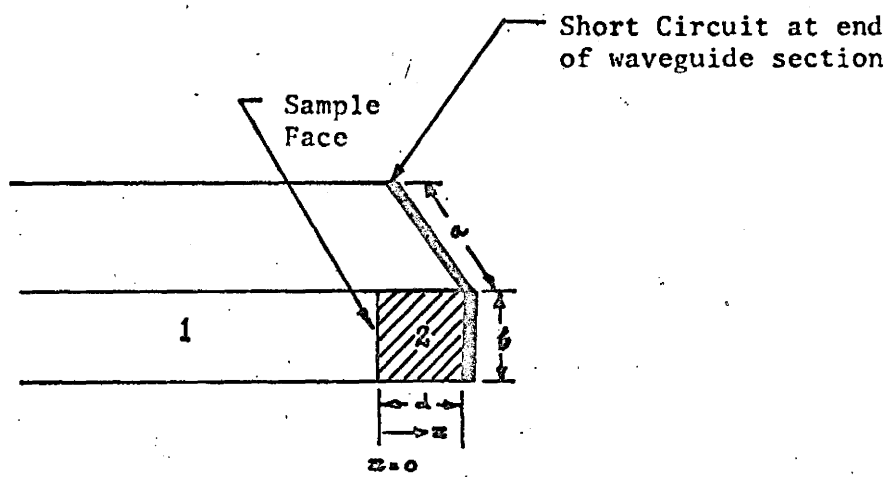

FIGURE 4: A waveguide section containing a semiconductor sample terminated by a short circuit.

Hence σ and ε_r can be found out if α, β are known. The values of α, β are, in fact, measured with a reflection bridge.

3.2 THEORY OF REFLECTION BRIDGE

Microwave bridges are most suitable for the precision measurement of the electrical properties (σ, ε) of solids. A general bridge (unmatched) can be used to obtain accurate results, provided the bridge is calibrated with three preliminary measurements.

CONSTRUCTION

The schematic diagram of a reflection bridge is shown in Fig. 5. The sample is coupled to one side arm and the precision short and attenuator in the other are adjusted until the output is minimized.

The hybrid 'tee' is converted into a magic 'tee' by inserting tuning slide screw tuners in E and H arms and also in side arms to compensate asymmetry. The magic 'tee' has the property that when the reflection co-efficients atreference planes in the side arms are equal, the power fed to the detector in the E arm is zero.

THEORY OF OPERATION[21]

The reflection co-efficient $\rho(x) = \rho_2 e^{2\gamma_s \ell_s}$ (3.5)

where ρ_2 = reflection co-efficient at Port 2

γ_s = prop. constant in the sample arm

ℓ_s = distance of measuring plane from Port 2.

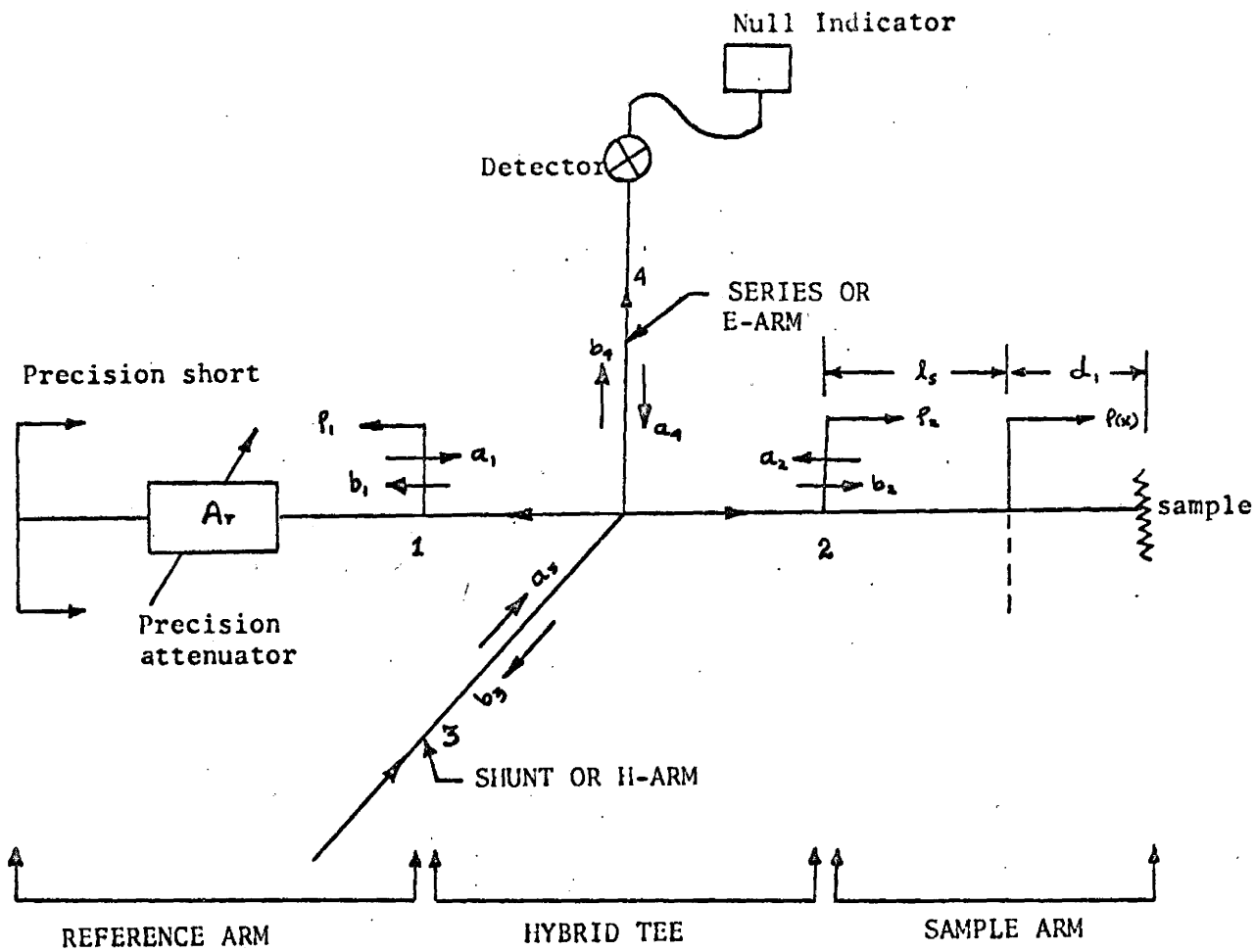

FIGURE 5: A microwave reflection bridge

Ports 1 and 2 are located in side arms and power enters through H arm.

For hybrid 'tee'

$$b = Sa$$

or

$$\begin{bmatrix} b_1 \\ b_2 \\ b_3 \\ b_4 \end{bmatrix} = \begin{bmatrix} S_{11} & S_{12} & S_{13} & S_{14} \\ S_{21} & S_{22} & S_{23} & S_{24} \\ S_{13} & S_{23} & S_{33} & S_{34} \\ S_{14} & S_{24} & S_{34} & S_{44} \end{bmatrix} \begin{bmatrix} a_1 \\ a_2 \\ a_3 \\ a_4 \end{bmatrix} \tag{3.6}$$

where a = incident wave

b = scattered wave

S = scattering matrix

Also,

$$\left.\begin{aligned} \rho_1 &= \frac{a_1}{b_1} \\ \rho_2 &= \frac{a_2}{b_2} \end{aligned}\right\} \tag{3.7}$$

Noting that $b_4 = a_4 = 0$ for null condition, one can obtain $\rho(x)$, after solving equations (3.5), (3.6) and (3.7) for ρ_2, as

$$\rho(x) = \frac{\rho_1 a - b}{\rho_1 c - 1} \tag{3.8}$$

where

$$a = \left[\frac{S_{11} S_{34} - S_{13} S_{14}}{S_{22} S_{34} - S_{23} S_{24}}\right] e^{2\gamma_s \ell_s} \tag{3.8(a)}$$

$$b = \left[\frac{S_{34}}{S_{22} S_{34} - S_{23} S_{24}}\right] e^{2\gamma_s \ell_s} \tag{3.8(b)}$$

and $$c = \left[\frac{(S_{11}\,S_{22} - S_{12}^{2})\,S_{34} + (S_{13}\,S_{12} - S_{23}\,S_{11})\,S_{24}}{S_{22}\,S_{34} - S_{23}\,S_{24}} + \frac{(S_{12}\,S_{23} - S_{13}\,S_{22})\,S_{14}}{S_{22}S_{34}S_{23}\,S_{24}}\right] \qquad (3.8(c))$$

The reflection co-efficient ρ_1 [21] of the reference arm has been shown to be equal to

$$\rho_1 = K\,e^{-2(A_r + j\,\beta_r \ell_r)} \qquad (3.9)$$

where $K = K_A K_S$, K_A = residual attenuation of the attenuator

K_S = zero setting and fixed loss of short circuit

A_r = reading of precision attenuator in neper

$\beta_r \ell_r$ = reading of precision short in radian

Equation (3.8) then reduces to

$$\rho(x) = \frac{A\,e^{-2(A_r + j\,\beta_r \ell_r)} - B}{C\,e^{-2(A_r + j\,\beta_r \ell_r)} - 1} \qquad (3.10)$$

where $A = aK$

$B = b$

$C = cK$

This is the general expression for the reflection co-efficient of the sample. The constants A, B, C can be determined by preliminary measurements, which constitute the calibration of the bridge.

(1) BRIDGE CALIBATION

Matched and symmetric bridge: when the bridge is matched and compensated for asymmetry,

$$S_{11} = S_{22},\quad S_{13} = S_{23},\quad S_{14} = -S_{24} \text{ and } S_{34} = S_{43} = 0,$$

Under these conditions, from equations (3.8(b)) and (3.8(c))

$$B = 0$$

$$C = 0$$

and equation (3.10) reduces to

$$\rho(x) = -A\, e^{-2(A_r + j\,\beta_r \ell_r)} \tag{3.11}$$

When a precision short circuit is placed at d_1,

$$\rho(s_1) = \rho(x)\, e^{2\gamma_s d_1}$$

$$\text{or } -1 = \rho(x)\, e^{2\gamma_s d_1}$$

$$\rho(x) = -e^{-2\gamma_s d_1}$$

By equation (3.11),

$$-e^{-2\gamma_s d_1} = -A\, e^{-2(A_r(s_1) + j\,\beta_r \ell_r(s_1))}$$

where $A_r(s_1)$ = Attenuator reading with a fixed short

$\beta_r \ell_r$ = Precision short reading with a fixed short

or
$$A = \frac{e^{-2\gamma_s d_1}}{e^{-2(A_r(s_1) + j\,\beta_r \ell_r(s_1))}}$$

Hence, by equation (3.11),

$$\rho(x) = -e^{-2[\{A_r - A_r(s_1)\} + j\,\beta_r\{\ell_r - \ell_r(s_1) + d_1\}]}$$

$$= -e^{-(A + j\,\phi)} \qquad (3.12)$$

where $A = 2\,\{A_r - A_r(s_1)\}$ in neper

$\phi = 2\,\beta_r\{\ell_r - \ell_r(s_1) + d_1\}$ in radian

The equation (3.12) has been used for this measurement of reflection co-efficient at the air-sample interface.

(2) MATCHED AND UNSYMMETRIC BRIDGE

If the input ports of hybrid 'tee' are matched and the bridge is not compensated for asymmetry, then $S_{11} = S_{22} = 0$

$S_{12} = S_{21} = 0$ at a single frequency

and by equation (3.8 (c)), $C = 0$, so that

$$\rho(x) = -A\,e^{-2(A_r + j\,\beta_r\ell_r)} + B \qquad (3.13)$$

(a) With a precision short circuit termination at the sample arm,

$$-e^{-2\gamma_s d_1} = -A\,e^{-2[A_r(s_1) + j\,\beta_r\ell_r(s_1)]} + B \qquad (3.13(a))$$

(b) With a matched termination Z_o at the sample arm,

$$0 = -A\,e^{-2[A_r(Z_o) + j\,\beta_r\ell_r(Z_o)]} + B \qquad (3.13(b))$$

Solving equations (3.13(a)), (3.13(b)) for A, B one can obtain $\rho(x)$ from equation (3.13),

$$\rho(x) = - \frac{e^{-2\gamma_s d_1}}{\left[1 - \frac{\rho_1(Z_o)}{\rho_1(s_1)}\right]} \left[e^{-2[A_r - A_r(s_1) + j\,\beta_r(\ell_r - \ell_r(s_1)]} - \frac{\rho_1(Z_o)}{\rho_1(S_1)}\right] \qquad (3.14)$$

where $$\frac{\rho_1(Z_o)}{\rho_1(s_1)} = \frac{e^{-2[A_r(Z_o) + j\,\beta_r \ell_r(Z_o)]}}{e^{-2[A_r(s_1) + j\,\beta_r \ell_r(s_1)]}}$$

The R. H. S. of equation (3.14) contains known quantities and enables $\rho(x)$ to be evaluated.

It is to be noted that equation (3.14) reduces to (3.12) provided $\frac{\rho_1(Z_o)}{\rho_1(s_1)} = 0$.

(3) GENERAL BRIDGE

It has been mentioned earlier that the reflection co-efficient for a general bridge is given by

$$\rho(x) = \frac{A\, e^{-2(A_r + j\,\beta_r \ell_r)} - B}{C\, e^{-2(A_r + j\,\beta_r \ell_r)} - 1}$$

where the values of the constants A, B, C can be determined by calibrating the bridge with two shorts at two different distances d_1, d_2 from

measuring plane and with one matched termination Z_o at the sample arm.

3.3 THEORY OF MEASUREMENT OF PROPAGATION CONSTANT[22]

The sample is placed at the end of a wave guide terminated by a short (Fig. 4). The input impedance at the air-sample interface $Z(o)$, obtained from the measurement of reflection co-efficient $\rho(o)$, is used to determine the propagation constant of the sample $\gamma = \alpha + j\,\beta$.

MEDIUM I

In medium 1, the reflection co-efficient at $z = 0$ is given by

$$\rho(o) = \frac{Z(o) - Z_1}{Z(o) + Z_1}$$ where Z_1 = impedance of the empty guide

or
$$Z(o) = Z_1 \frac{1 + \rho(o)}{1 - \rho(o)}$$
$$= Z_1 \frac{1 - e^{-(A + j\,\phi)}}{1 + e^{-(A + j\,\phi)}} \qquad (3.15)$$

where A, ϕ are twice the readings between the attenuation in neper and phase shift in radian respectively (readings with the sample and short and with the short alone).

MEDIUM 2

In medium 2, the transverse components of electric and magnetic fields are:

$$E(z)_2 = E_{i_2}\, e^{-\gamma_2 z} + E_{r_2}\, e^{\gamma_2 z} \qquad (3.16)$$

$$H(z)_2 = \frac{E_{i_2}}{Z_2} e^{-\gamma_2 z} - \frac{E_{r_2}}{Z_2} e^{\gamma_2 z} \tag{3.17}$$

where E_{i_2}, E_{r_2} are amplitudes of incident and reflected waves.

Since the guide is terminated by a short at z = d, by equation (3.16),

$$0 = E_{i_2} e^{-\gamma_2 d} + E_{r_2} e^{\gamma_2 d}$$

or

$$\frac{E_{r_2}}{E_{i_2}} = - e^{-2\gamma_2 d} \tag{3.18}$$

Using equations (3.16), (3.17) and (3.18),

$$E(o)_2 = E_{i_2} [1 + (-e^{-2\gamma_2 d})]$$

$$H(o)_2 = \frac{E_{i_2}}{Z_2} [1 - (-e^{-2\gamma_2 d})]$$

$$Z(o) = \frac{E(o)_2}{H(o)_2}$$

$$= Z_2 \tanh (\gamma_2 d)$$

$$= Z_1 \frac{\gamma_1}{\gamma_2} \tanh (\gamma_2 d) \tag{3.19}$$

Since for a TE wave,

$$\frac{Z_2}{Z_1} = \frac{\frac{j\omega\mu_2}{\gamma_2}}{\frac{j\omega\mu_1}{\gamma_1}} .$$

Equating (3.15) and (3.19) one can obtain,

$$\frac{\tanh(\gamma_2 d)}{\gamma_2 d} = \frac{1}{j\beta_o d}\,\frac{1 - e^{-(A + j\phi)}}{1 + e^{-(A + j\phi)}}$$

$$= \frac{1}{j\beta_o d}\,|Z_n|e^{j\theta}$$

$$= C_s \angle -\S \qquad (3.20)$$

where
$$|Z_n| = \left[\frac{\cosh A - \cos\phi}{\cosh A + \cos\phi}\right]^{1/2} \qquad (3.21)$$

$$\theta = \tan^{-1}\left[\frac{\sin\phi}{\sinh A}\right] \qquad (3.22)$$

$$C_s = \frac{|Z_n|}{\beta_o d} \qquad (3.23)$$

$$\S = \frac{\pi}{2} - \tan^{-1}\left[\frac{\sin\phi}{\sin hA}\right] \qquad (3.24)$$

where equation (3.21) and (3.22) are found in literature[23]. The C_s and § can be found by measuring the sample thickness, the wavelength λ in the empty guide and the value of A and ϕ with a reflection bridge.

The next step is to determine

$$\frac{\tanh T e^{j\tau}}{T e^{j\tau}} = C_s e^{-j\S} \text{ from the graphs of von Hippel}^{(22)}$$

where

$$\gamma_2 = \frac{T e^{j\tau}}{d}$$

$$\text{when } \alpha = \frac{T}{d}\cos\tau \qquad \} \qquad (3.25)$$

$$\beta = \frac{T}{d}\sin\tau$$

Once α, β are known, the resistivity and dielectric constant are evaluated from equations (3.3) and (3.4).

CHAPTER IV

EXPERIMENTAL PROCEDURES

4.1 (a) PREPARATION OF SAMPLES

The samples of germanium in the form of rectangular pieces were cut from a large block of 10 ohm-cm. n-G_e <111> crystal by means of a 20 mils thick diamond wheel cutter. The samples were cut 2 to 3 mils oversize and then polished with silicon carbide paper by hand with care, so that all edges of the sample remained perpendicular to each other. The thickness of the sample was chosen to obtain maximum accuracy of measurement and minimum loss and was kept at least equal to the skin depth. The skin depth δ was calculated for ρ = 10 ohm-cm., f = 9.522 GHz from the expression

$$\delta = \frac{1}{\sqrt{\pi f \mu_o / \rho}} = 0.063"$$

The measurement accuracy is a maximum[22] when the sample thickness

$$\ell = \frac{\lambda g}{4}, \; 3\frac{\lambda g}{4}, \; 5\frac{\lambda g}{4} \text{ etc.}$$

To have minimum loss, ℓ was chosen to be one quarter wavelength in the sample

$$\ell = \frac{\lambda g}{4} = \frac{\pi}{2\beta}$$

where β = phase constant of the sample, which was obtained from equation (3.2)

$$\gamma^2 = \left(\frac{\pi}{a}\right)^2 - \omega^2 \mu_o \varepsilon_o \varepsilon_r + j\omega\mu_o\sigma$$

$$= 1.89 - 63.5 + j\frac{790}{\rho} \qquad \text{for } \varepsilon_r = 16$$

$$= 100 \angle 128^\circ \qquad f = 9.522 \text{ GHz}$$

$$\rho = 10 \text{ ohm-cm.}$$

$$\gamma = 4.38 + j8.987 \text{ /cm.}$$

$$= \alpha + j\beta$$

$$\text{when } \ell = \frac{\pi}{2\beta} = 0.069"$$

Since $\frac{\lambda g}{4} \approx \delta$, the length of the sample was chosen equal to skin depth (63 mils).

N-type germanium of resistivity 10 ohm-cm. was chosen, because

(i) it shows hot electron effects

(ii) it is suitable for measurement with a reflection bridge

(iii) it has low joule heating for the large samples required for 10 GHz measurements

However, it is difficult to make non-injecting contacts, to such high resistivity material because the critical current density at which injection starts is lower for a high resistivity sample[6, 11].

(b) PREPARATION OF NON-INJECTING CONTACTS[24, 25]

All faces of the samples were polished with emery paper and then cleaned by etching for 30 secs. either in Hydrogen Peroxide or in an etching solution, which contains[25]:

3 parts HNO_3 (sp. gr. 1.42)

2 parts H_2O (dimineralized)

1 part HF (40%)

Using polyflux, the specimen was then soldered with a solder ($95\%S_n + 5\%S_b$) containing impurity of the same type as in the body of the semiconductor and at a temperature of about 300°C. During the high temperature cycle of soldering operation, enough of the material from the molten solder diffused into the surface layer of the semiconductor producing a heavily doped region (Fig. 6). This region provides recombination centres for any minority carriers injected during the application of a potential across the sample.

Precautions

(i) Care should be taken to ensure that the solder covers the whole face of the sample.

(ii) Excess solder, which may run over to adjacent faces, should be removed by polishing.

(iii) Large specimens can be used to reduce errors due to injection. Also, minority carriers, if injected in pulses of short enough duration, do not have enough time to modulate the conductivity

of the main section.

(iv) Short pulses can be used to avoid surface breakdown.

Proof of Non-injection

The change of resistance measured by a Wheatstone bridge for opposite directions of current flow across the junction can be measured. For the samples prepared this was not greater than 0.2% strongly suggesting that the contacts are non-rectifying and non-injecting.

Another indication of an injecting contact is a rise of current with voltage over the period of an applied pulse. This may occur due to hole injection or from surface generation. This effect was only observed in the samples prepared for electric fields outside the range of interest (0 - 3KV/cm.).

4.2 MEASUREMENT OF CARRIER DRIFT VELOCITY

The drift velocity of electrons in the 10 ohm-cm. n-G_e samples was measured as a function of electric field. The experimental arrangement is shown in Fig. 7.

(a) PULSE GENERATOR

To avoid joule heating in the sample, pulsed electric field of duration 0.5-1.5 μ sec. with a repetition rate 1 p/s was used. This necessiated the assembling of a pulse generator and a hydrogen thyratron on-off pulse generator[26], which was available, was converted into a line type pulse generator[27]. This type of pulse generator was chosen to

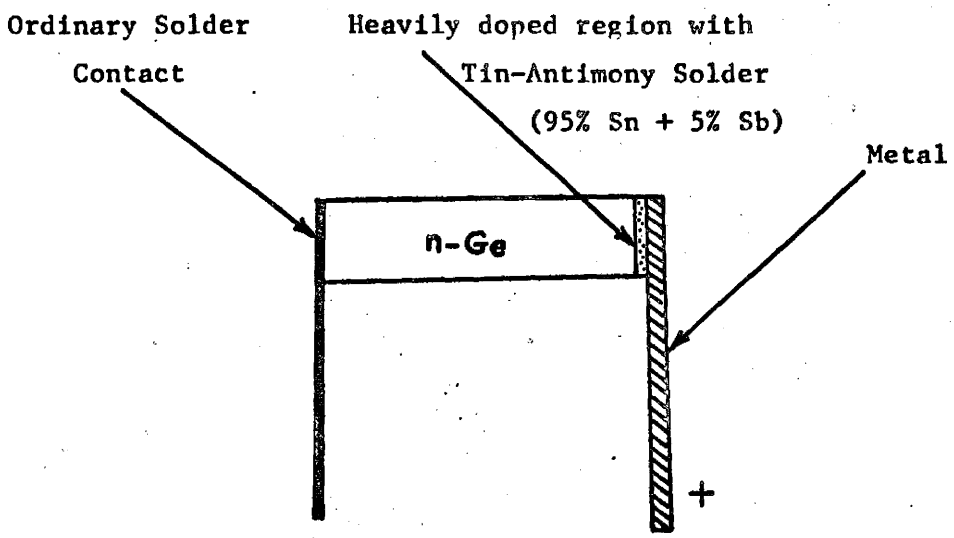

FIGURE 6: A non-injecting contact

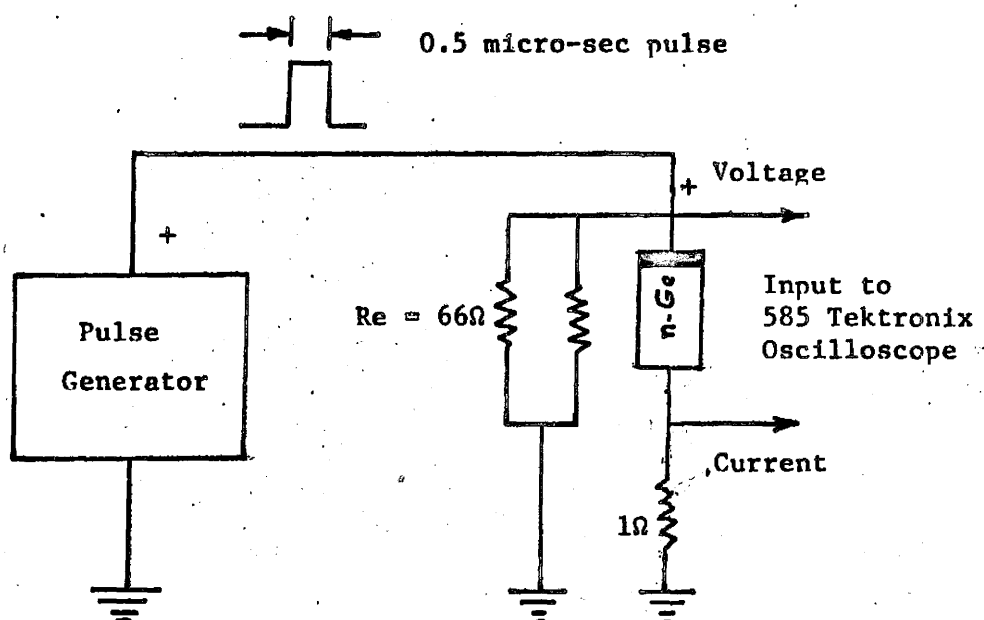

FIGURE 7: An arrangement for drift velocity measurement.

obtain a well shaped rectangular pulse and has the advantage of little likelihood of accidental damage to the load in the case of malfunction as all the energy stored in the cable is discharged in each pulse.

The ratings of the pulse generator used were:

voltage: 0 - 8KV	Thyratron r_p: 2 ohm
Duration: 0.5 - 1.5 μ sec.	Ionisation time: 0.05 μ sec.
r.p.r.: 1 p/s	De-ionisation time: few μ secs.
Source imped: 50 ohm	Trigger voltage: 200 - 300V

(b) MEASURING PROCEDURE[3, 5, 6]

The sample was first matched to the pulse generator by means of a parallel chain of resistors to ensure a single well shaped rectangular pulse. The current through the specimen was measured by measuring the voltage across the 1 ohm (.1%) resistor. The voltage across the specimen was measured independently. Both current and voltage measurement were taken with a 585 Tektronix oscilloscope.

The drift velocity was calculated from the expression

$$v = \mu_o \frac{R_o I}{L} \qquad (4.1)$$

where μ_o = low field mobility $(\frac{cm.^2}{V\text{-}sec.})$

R_o = low field resistance (ohm)

L = length of the specimen in cm.

I = current through the sample in amp.

4.3 MEASUREMENT OF CONDUCTIVITY AND DIELECTRIC CONSTANT

(a) DESCRIPTION OF CIRCUITS AND APPARATUS

A schematic diagram for the measurement of propagation constant $\gamma = \alpha + j\beta$ with a reflection bridge is shown in Fig. 8. The equipment used is as follows:

(i) Klystrons

The klystron used as a signal source is an X-13 reflex type, with a frequency range of 8.2 - 12.4 GHz which can be varied by a micrometer adjustment. The maximum power for optimum load is 750 mw. The power to the klystron was supplied from the P. R. D. power supply, type 809A.

The klystron used for the local oscillator is a type 2K25 with a frequency range 8.5 - 9.66 GHz and 30 mw power output. Power to this klystron was supplied from an FXRZ815B Universal Klystron Power Supply.

(ii) Ferrite Isolators

A undirectional element is used to isolate klystron from the rest of the circuit. For transmission in the forward direction, the isolator has practically zero attenuation but for reverse direction, it has approximately 30 db attenuation. Units manufactured by P. R. D. were used in the bridge assembled.

FIGURE 8: An experimental setup of a reflection bridge

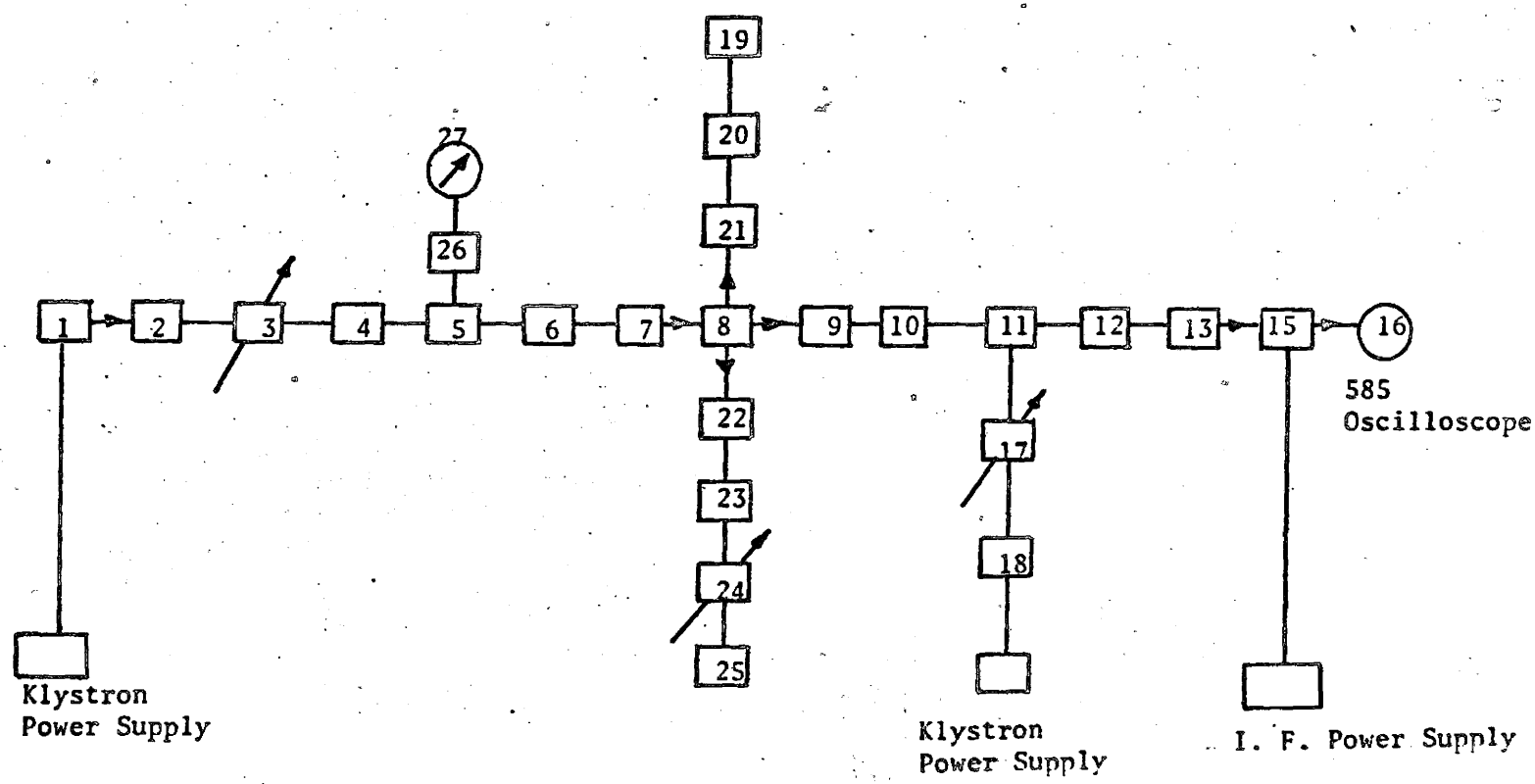

1. Klystron X-13
2. Isolator
3. Attenuator
4. Wavemeter
5. Directional Coupler
6. SW Indicator
7. Tuner
8. Hybrid tee
9. Isolator
10. Tuner
11. Directional Coupler
12. Isolator
13. Matched Detector
15. I. F. Amplifier
16. 585 Oscilloscope
17. Variable attenuator
18. Local Klystron Oscillator
19. Sample holder
20. 0.5 db attenuator
21. Tuner
22. Tuner
23. Tuner
24. Precision attenuator
25. Precision Short
26. Detector
27. Indicator

(iii) Variable Attenuator

This is used to control the power input to the circuit and again a P. R. D. unit was used.

(iv) Hybrid Tee, Precision Attenuator And Precision Short

High quality equipment is required for these components. Elliott instruments are used for the attenuator and short circuit and the hybrid tee was manufactured by Demornay Bonardi.

(v) Sample Holders

Sample holders were machined from standard x-band wave guide as shown in Fig. 9. The configuration of Fig. 9(a) with the semiconductor placed fully inside the sample holder was used for the basic measurements of ρ and ϵ_r.

The slotted holders shown in figures 9(b) and 9(c) were used for high field measurements. The slots were cut slightly oversize to provide polythene insulation (9 mils thick) between the sample and the holder.

The unslotted holders are shown in Fig. 9(d) and 9(e) were also used for high field measurements. The samples were placed at the end of the guide and backed with a short circuiting plate. This arrangement has fewer insulation problems than the configuration of Figs. 9(b) and 9(c) and has the advantage of ease of rotation of the sample position with respect to guide.

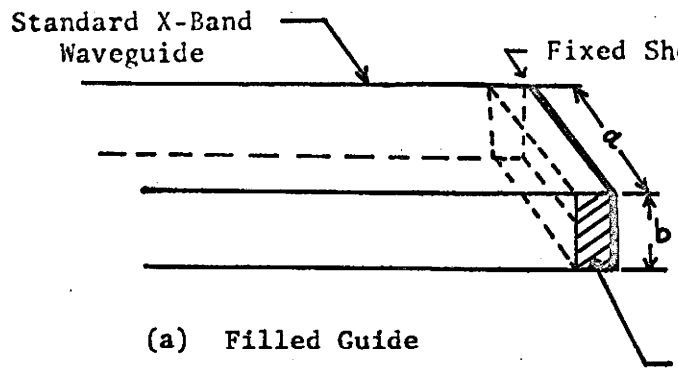

(a) Filled Guide

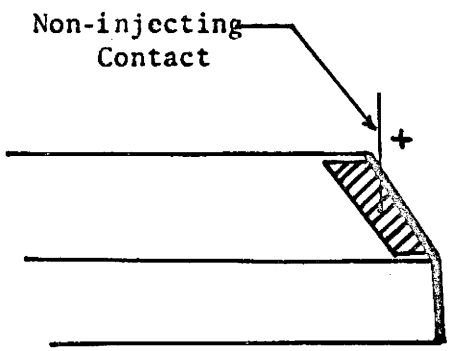

(b) Semiconductor mounted in slot in broad wall of guide

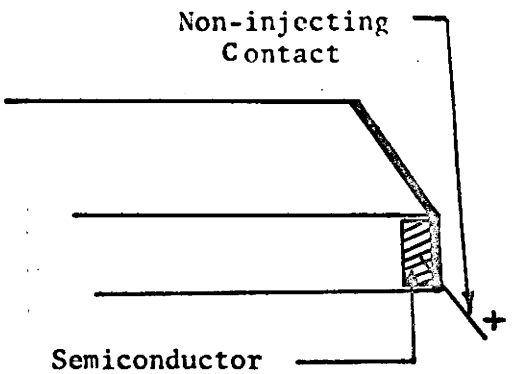

(c) Semiconductor mounted in slot in narrow wall of guide

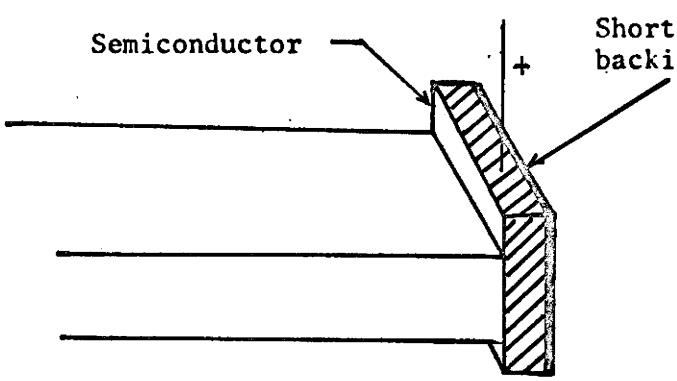

(d) Unslotted Guide: Parallel Applied Fields

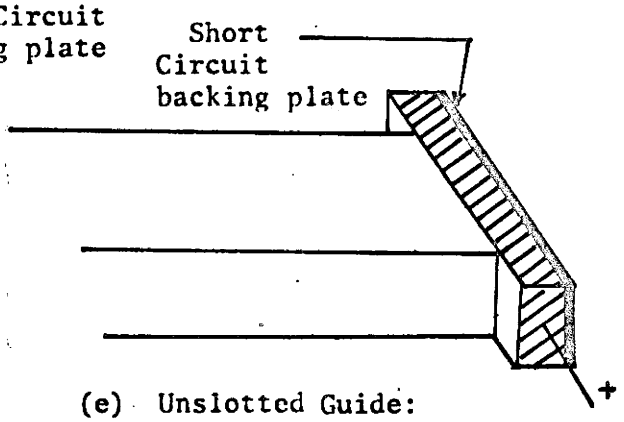

(e) Unslotted Guide: Perpendicular Applied Fields

FIGURE 9: Semiconductor Sample Holders. The samples in (b), (c), (d) and (e) are insulated from the guide walls with polyethelene film.

(vi) Matched Detector

The crystal detector using a crystal type IN23B is matched by an adjustable screw tuner as well as by a variable short, for maximum output. The output of the crystal (.5MA) is varied by changing the output of the local oscillator.

(vii) I. F. Amplifier

The I. F. amplifier has a bandwidth of 20 MC/s., centered at 30 MC/s and an adjustable gain to 45 db. The output resistance of the source (crystal mixer) is a function of rectified current depending on the output of the local oscillator, while the input resistance of the I. F. amplifier is 300 ohm.

An attenuator circuit was built to match the crystal detector to the I. F. amplifier. The connecting lead (93 ohm coaxial cable) was kept as short as possible and the output of the final stage of the amplifier, which consists of a diode with a 16 KΩ load followed by a cathode follower of low output impedance, is fed directly into the d.c. input of 585 oscilloscope. Variations in the output of the detector are therefore recorded as d.c. changes on the oscilloscope.

(b) MEASURING PROCEDURES

The measurements were made at a frequency of 9.522 GHz and the setting up procedure was as follows:

(i) The hybrid 'tee' was matched in E and H arm with tuning

screws after terminating the two side arms in matched loads. The bridge was then balanced for minimum output by adjusting tuning screw in the reference arm, while a well matched sliding termination was coupled to sample arm. When the output was unaffected by varying the positions of the sliding match, the asymmetry in the Hybrid tee had been compensated.

(ii) The precision attenuator was then matched with another tuner, which was adjusted for minimum output. The performance of the bridge was then described by equation (3.12) and it was ready for measurement.

The sample arm was first shorted by a fixed short circuit plate and the precision attenuator and the precision short were then adjusted for minimum output. Their readings A_o, ℓ_o were noted. The short was then replaced by the sample backed with another short circuit plate and the readings A_1, ℓ_1 were recorded. Care was taken to position the sample faces normal to the axis of the guide.

With an applied pulsed electric field to the sample, the amplified detector output, during the period of the 0.5 μ sec. pulse, appears on the 585 Tetronix Oscilloscope due to the hot electron effect. The precision attenuator and short were then adjusted to bring the top of the pulse as near to the balanced zero position as possible. The best balance conditions applied when the pulse deration was increased to 1.5 μsec. Measurements were made with both 0.5 and 1.5 sec. pulses for applied fields, up to 3KV/cm.

One important phenomenon, that was observed during the experiment, was the noise pick up by I. F. amplifier from the discharge of the thyratron tube. This was finally avoided by completely screening the I. F. amplifier, using shortest possible co-axial leads and decoupling the power supply to I. F. amplifier.

(c) SOURCES OF ERROR

The important sources of errors in the experiments are

(i) Observational errors in A_o, A_1 and ℓ_o, ℓ_1

A 1% change in A can cause about 1% change in resistivity and a 1% change in ϕ can cause about 1% change in resistivity.

(ii) Errors in reading the value of T and τ from the graphs of von Hippel.

A 1% change in T and τ can cause about 1% and 2% changes in resistivity respectively.

(iii) Errors in calculating $\frac{\nu}{E}$ and $\frac{\partial \nu}{\partial E}$. The error in measuring drift velocity is about 2% and a 2° variation of the slope of the ν-E curve can cause about a 2% change in $\frac{\partial \nu}{\partial E}$.

(iv) Non-uniformity of the sample resistivity. The 4 point probe measurements showed variations about 1% in resistivity over the surface of the sample.

4.4 MEASUREMENT OF D. C. RESISTIVITY

There are various methods of measuring the d.c. resistivity of semiconductors. The four point probe method is a well known one and has the advantage that it does not require any specific shape of the sample.

In this method, four probes are placed on the flat surface of the sample and current is passed through the outer probes and the voltage V is measured between the inner probes. The conductivity σ is then given by[28]

$$\sigma = \frac{I}{2\pi V}\left[\frac{1}{S_1} + \frac{1}{S_3} - \frac{1}{S_1+S_2} - \frac{1}{S_1+S_3}\right] \qquad (4.2)$$

where S_1, S_2 and S_3 are probe spacings.

When the probe spacings are equal, the resistivity, ρ

$$\rho = 2\pi S \frac{V}{I} \qquad (4.3)$$

Equation (4.3) was used to calculate the d.c. resistivity of the sample. The results are tabulated in Table 5.5.

The following precautions are required for the use of this method:

(i) If the dimensions of the sample are small compared to probe spacing, the corrections shown in Fig. 10 must be applied.

(ii) The edge of the sample must be at least a distance 3S away from the probe.

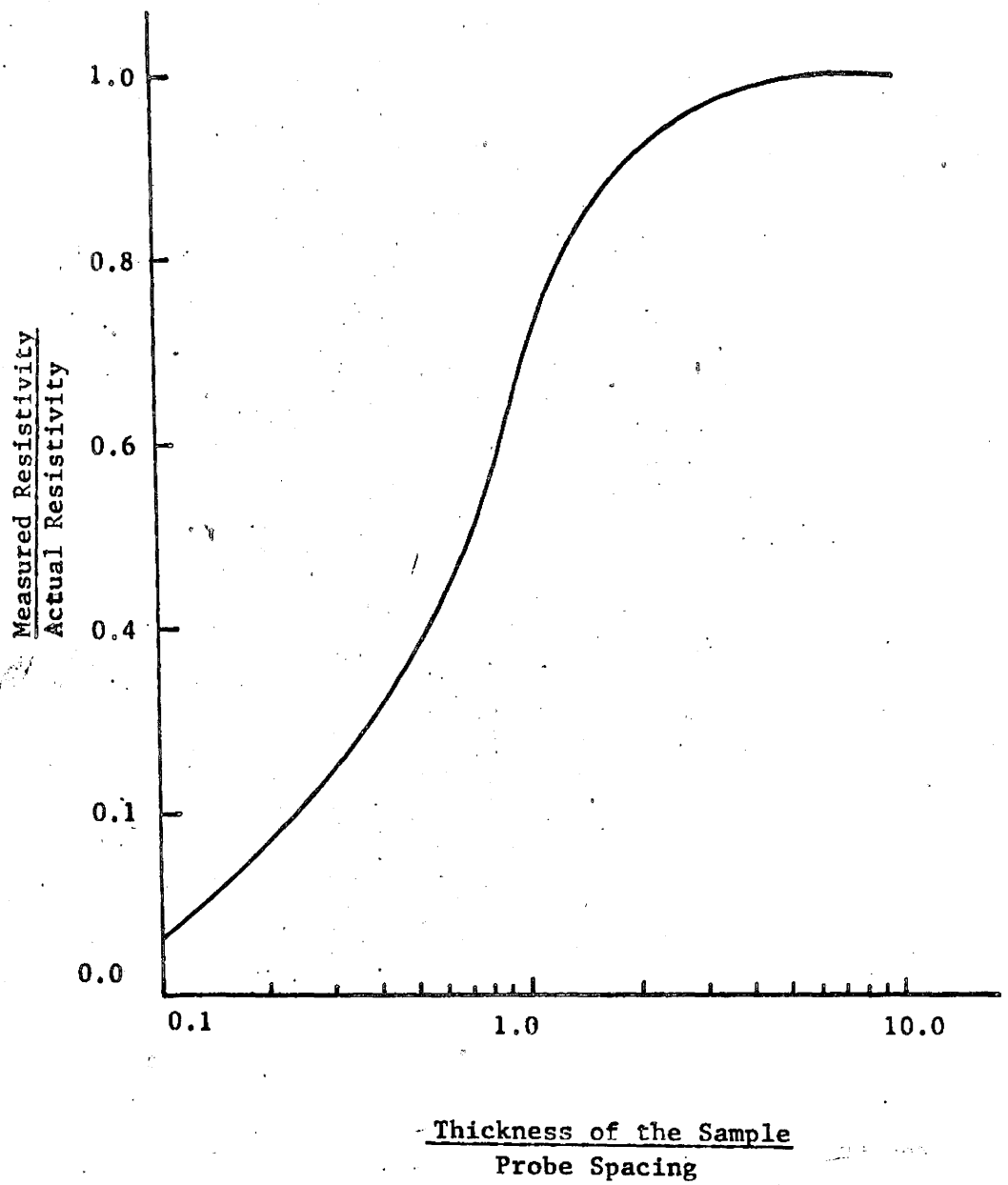

FIGURE 10: Four Probe Resistivity Correction Curve (after Hunter [29])

(iii) The sample should be homogeneous.

(iv) For accurate measurements, the current should be small and supplied from a constant current source to reduce the the contact problem.

(v) Measurements should be taken for both forward reverse direction of current flow to avoid errors due to dis-symmetry of contacts.

CHAPTER V

RESULTS

5.1 MEASUREMENT OF DRIFT VELOCITY

Measurements of the electron drift velocity in an n-type germanium sample as a function of applied electric field are given in Table 5.1. The sample resistivity was ρ = 10 ohm-cm., length = 2.87 cm., and low field resistance = 195 ohm.

The applied d.c. pulse duration was .5 - 1.5 μ sec.

Table 5.1

Electric Field in KV/cm.	Current Through the Sample in Amp.	Drift Velocity of Electrons in cm./sec.
0.453	7.5	1.93×10^6
0.68	10.5	2.71×10^6
1.05	15.0	3.87×10^6
1.26	16.0	4.13×10^6
1.92	21.2	5.48×10^6
2.01	21.8	5.5×10^6
2.75	24.4	6.7×10^6

These results are plotted in Figure 11 and d.c. and differential mobilities deduced graphically from Figure 11 are shown in Figure 12 by solid lines.

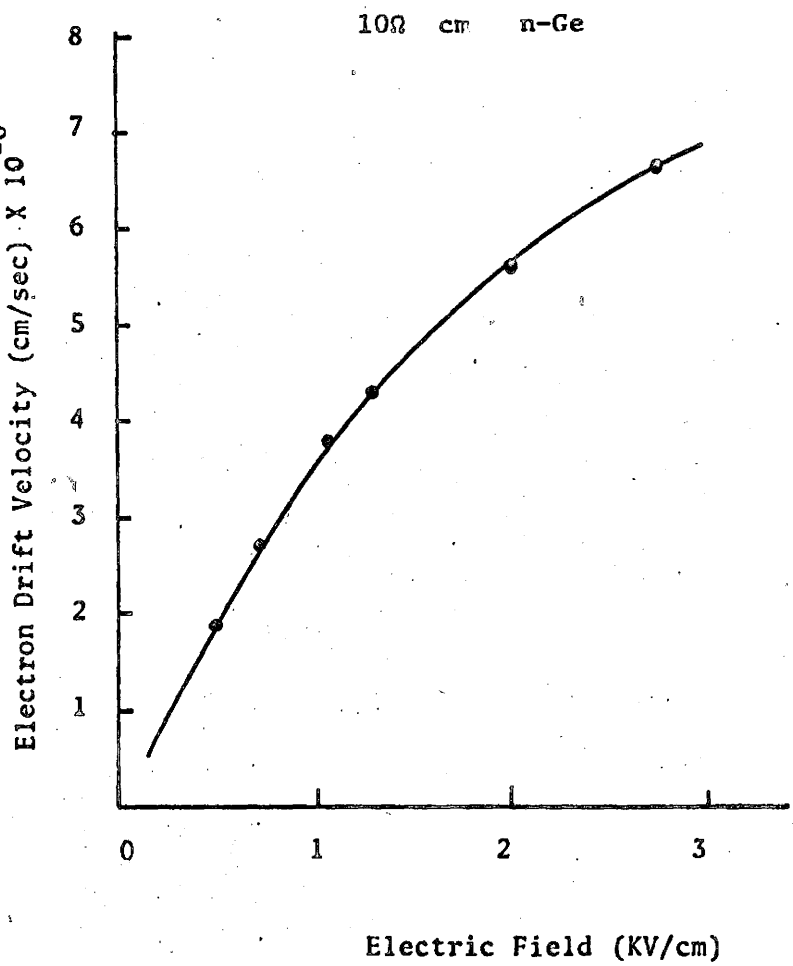

FIGURE 11: Variation of electron drift Velocity with Electric Field

5.2 MICROWAVE MEASUREMENT OF ρ AND ϵ_r

(a) MEASUREMENT WITH ZERO APPLIED FIELD

Measurements at a frequency 9.522 GHz (β_o = 1.45 rad/cm.) on semiconductor samples mounted in completely filled, slotted and unslotted guides are given in Table 5.2.

(b) MEASUREMENT IN UNSLOTTED WAVE GUIDE WITH APPLIED FIELDS 0 - 3KV/cm

(i) Measurements for the conditions of parallel microwave and applied field vectors with

$$f = 9.522 \text{ GHz}, \ \beta_o = 1.45 \text{ rad/cm.}, \ d = 0.1626 \text{ cm.}$$

$$A_o = 0.10 \text{ db}, \ \ell_o = 1.687 \text{ cm.}, \ d_1 = 0.000 \text{ cm.}$$

are given in Table 5.3.

It will be noted that the presence of the insulation and airgap has decreased the resistivity by about 30% from the absolute value and increased the dielectric constant by almost 80% compared with the values measured in the completely filled guide. However, the absolute values of resistivity are not required as the comparison between theory and experiment is made on the basis of relative changes in the sample conductivity.

(ii) Measurements for the condition of applied microwave and applied electric field vectors at right angles with

$$f = 9.522 \text{ GHz}, \ \beta_o = 1.45 \text{ rad/cm.}, \ d = 0.1600 \text{ cm.}$$

$$A_o = 0.15 \text{ db}, \ \ell_o = 1.667 \text{ cm.}, \ d_1 = 0.00$$

are given in Table 5.4.

The conductivity for parallel fields marked (x,•) and that for perpendicular fields marked (■,Δ) measured at 9.522 GHz are shown in Figure 12. All values are normalized by taking the zero field as unity. The attenuation and phase changes for the parallel and perpendicular conditions of applied fields are shown in Figure 13.

5.3 MEASUREMENT OF D. C. RESISTIVITY

Measurements of the d.c. resistivity of the sample by means of the 4 probe method are given in Table 5.5. For these measurements $\frac{\text{Sample Thickness}}{\text{Probe Spacing}} = 1.27$, the approximate correction factor = 0.81.

MEASUREMENT WITH ZERO APPLIED FIELD

Table 5.2

Wave Guide Structure	A_o db	ℓ_o cm	A_1 db	ℓ_1 cm	d_1 cm	C_s §	T τ	α nep/cm	β rad/cm	ρ ohm-cm	ε_r
Fig. 9(a) Sample	0.00	1.684	1.82	1.813	0.000	1.232 49.84	1.45 67.50	3.53	8.53	12.4	15.6
Thickness d=0.157 cm.	0.04	1.713	1.85	1.691	0.157	1.255 48.45	1.42 67.7	3.43	8.37	13.1 av. 12.75	15.1 av. 15.35
Fig. 9(b) d=0.1346	0.19	1.698	1.71	1.878	-0.086	1.312 53.23	1.5 65.5	4.62	10.14	8.0	20.9
Fig. 9(c) d=0.1448	0.04	1.432	3.3	1.614	-0.0976	1.809 73.66	1.58 76.5	2.55	10.61	13.9	27.1
Fig. 9(d) d=0.1626	0.10	1.687	1.85	1.689	0.000	0.846 89.2	1.95 71.5	3.80	11.37	8.7	29.3
Fig. 9(e) d=0.1600	0.15	1.667	1.78	1.680	0.000	0.806 84.4	1.94 69.9	4.17	11.39	7.9	28.7

MEASUREMENT IN UNSLOTTED WAVE GUIDE WITH PARALLEL MICROWAVE AND APPLIED ELECTRIC FIELD VECTORS

Table 5.3

Pulse Duration (μ sec.)	E KV/cm	A_1 db	ℓ_1 cm	C_s §	T τ	α nep/cm	β rad/cm	$\rho_{\parallel}$ ohm/cm	$\varepsilon_{r_{\parallel}}$
No Pulse	0	1.85	1.689	0.846 89.2	1.95 71.5	3.80	11.37	8.7	29.3
0.5	0.94	3.06	1.712	1.404 84.4	1.70 74.9	2.72	10.09	13.7	24.2
	1.61	4.14	1.843	2.079 67.87	1.54 78.2	1.94	9.27	20.9	21.1
	2.55	5.72	1.903	2.738 70.92	1.53 81.2	1.44	9.30	28.0	21.7
	3.36	4.89	1.927	2.588 64.54	1.52 80.8	1.49	9.23	27.2	21.3
1.5	0.94	3.91	1.797	1.878 72.56	1.57 77.2	2.14	9.42	18.7	21.6
	1.61	4.38	1.812	2.100 72.12	1.55 78.50	1.91	9.37	21.0	21.6
	2.955	5.43	1.909	2.677 69.04	1.55 81.3	1.44	9.42	27.7	22.2

MEASUREMENT IN UNSLOTTED WAVE GUIDE WITH PERPENDICULAR MICROWAVE AND APPLIED ELECTRIC FIELD VECTORS

Table 5.4

Pulse Duration (μ sec.)	E KV/cm	A_1 db	ℓ_1 cm	C_s & §	T & τ	α nep/cm	β rad/cm	$\rho_\perp$ ohm-cm.	$\varepsilon_{r_\perp}$
No Pulse	0	1.78	1.680	0.806 84.4	1.94 69.9	4.17	11.39	8.0	28.7
0.5	0.77	2.08	1.693	0.959 80.72	1.84 70.1	3.91	10.81	8.9	26.0
	1.152	2.50	1.737	1.223 70.52	1.65 71.4	3.29	9.77	11.67	21.7
	1.554	2.86	1.663	1.307 90.99	1.75 75.8	2.68	10.60	13.2	26.9
1.5	0.27	1.93	1.683	0.8795 83.74	1.89 70.0	4.04	11.1	8.4	27.3
	1.35	2.86	1.760	1.930 68.2	1.59 72.2	3.04	9.46	13.1	20.6

MEASUREMENT OF D.C. RESISTIVITY

Table 5.5

No. of Observation	Direction of Current flow	Position of the probe	Voltage drop between inner probes in Volt	Current thru the sample in mA	Resistivity ρ in ohm-cm.
1	Forward	Parallel to sample length	0.0045	0.25	14.4
2	Forward	Parallel to sample length	0.0053	0.295	14.4
3	Reversed	Parallel to sample length	0.00635	0.44	14.5
4	Reversed	Perpendicular to sample length	0.0080	0.475	14.5
5	Reversed	Perpendicular to sample length	0.00855		14.4

Average resistivity = 14.44 ohm-cm.

Corrected resistivity = 11.65 ohm-cm.

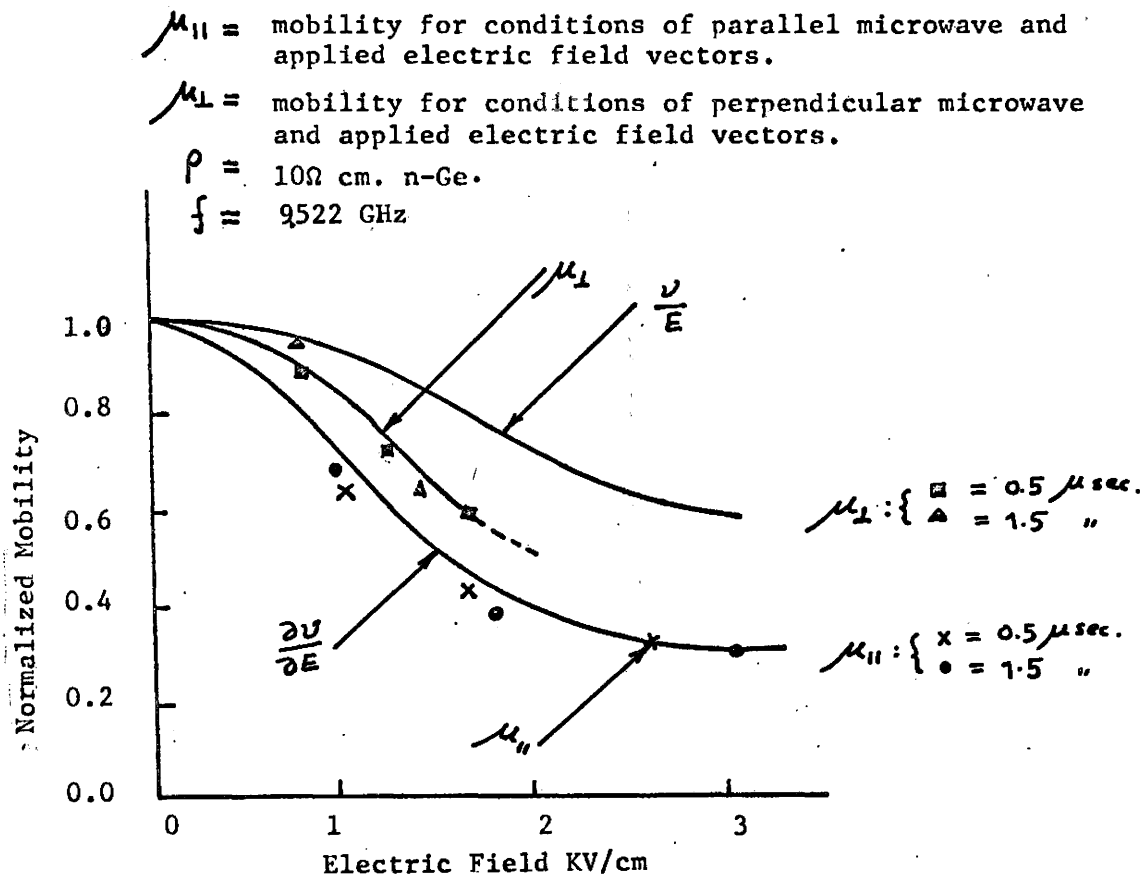

FIGURE 12: Variation of DC $(\frac{v}{E})$, differential $(\frac{\partial v}{\partial E})$ and microwave mobilities with electric field.

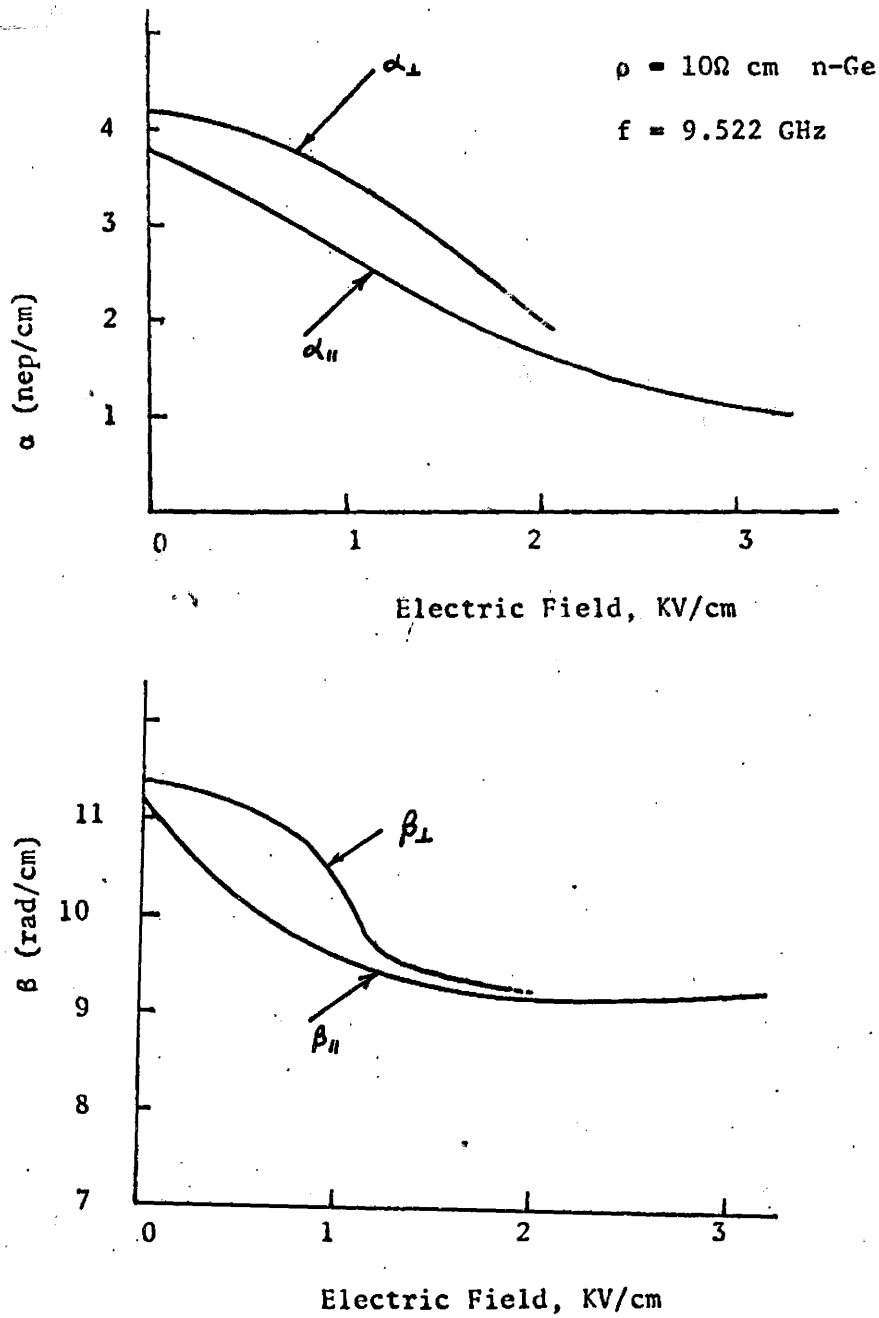

FIGURE 13: Variation of propagation constant $\gamma = \alpha + j\beta$ with Electric Field

CHAPTER VI

DISCUSSION

6.1 MEASUREMENTS OF RESISTIVITY AND DIELECTRIC CONSTANT

The value of resistivity supplied by the manufacturer was 10 ohm-cm. while that obtained by microwave measurement was 12.75 ohm-cm.. (Table 5.2). This disagreement necessiated the measurement of resistivity with a d.c. technique. For this purpose, the 4 point probe method (Section 4.4) was used. The value of resistivity obtained by this method was 11.65 ohm-cm. (Table 5.5) which was in closer agreement with the microwave measurements. Possible reasons for the difference (9%) in the d.c. and microwave measurements are the inhomogeneity of the sample and inaccuracies in the d.c. measurement due to the small size of the samples compared with the probe spacing.

The absolute dielectric constant obtained by microwave measurement was 15.35 (Table 5.2). This gives a measured value of the electronic contribution to the dielectric constant* of 16.0 - 15.35 = 0.65. It may be noted that the calculated value of the electronic contribution for 12.75 ohm-cm. germanium with a relaxation time $\tau = 5 \times 10^{-13}$ sec. is $\frac{\sigma_o \tau}{\varepsilon_o} = 0.443$.

---

* $\varepsilon_r = 16.0$ for intrinsic Ge obtained from infra-red measurements as reported in literature[19].

6.2 EFFECT OF SLOTS AND INSULATION

The resistivity measured (12.75 ohm-cm. Table 5.2) in the completely filled guide shown in Figure 9(a) is in reasonable agreement with that measured (13.9 ohm-cm. Table 5.2) in the slotted guide structure shown in Figure 9(c). This could be expected because the slot is normal to the broad wall of the wave guide.

However, the dielectric constant is increased by about 70% in this measuring configuration because of the presence of insulation (polythene) required around the sample to allow the application of large d.c. electric fields.

The percentage increase of the dielectric constant from the absolute value was found to depend on the thickness of the insulation. This can be seen from a set of results obtained experimentally with the wave guide structure of Fig. 9(c).

Insulation Thickness	ρ(ohm-cm.)	ε_r
0 inch	13.6	17.2
0.009 inch	13.9	20.6
0.018 inch	14.4	25.2

The resistivity and dielectric constant measured with the wave guide structure shown in Figure 9(b) were ρ = 8.0 ohm-cm., ε_r = 20.9 (Table 5.2) respectively. This mounting configuration thus results

in an apparent decrease of resistivity of about 33% and an increase of dielectric constant of about 32%. This could be expected, since the slot in the broad wall normal to the narrow wall, cuts the current lines and disturbs the field greatly.

For the unslotted guides of Figures 9(d) and 9(e), the resistivities measured were ρ = 8.7 and 7.9 ohm-cm. respectively (Table 5.2). The corresponding dielectric constants measured were ε_r = 29.3, 28.7 (Table 5.2). These results are in close agreement with those of Figure 9(b). This could be expected since the unslotted guides are comparable to the guide structure shown in figure 9(b).

6.3 HIGH ELECTRIC FIELD MEASUREMENTS

The measured microwave conductivity for the conditions of parallel microwave and applied electric field vectors, marked (x,•) in Figure 12, gave a normalized carrier mobility, which agreed well with the values of differential mobility $\frac{\partial v}{\partial E}$ obtained graphically from Figure 11.

These results confirm the measurements performed by Gunn[14] for the parallel field case with a transmission bridge.

However, the mobility derived for the conditions of perpendicular microwave and applied electric field vectors marked (■,Δ) in Figure 12 can be seen to be intermediate between the $\frac{\partial v}{\partial E}$ and $\frac{v}{E}$ curves, which were derived from Figure 11. The measurement of conductivity for this case was limited to 1.6 KV/cm. because of the large sample

length required and the consequent sparking and surface breakdown problems encountered.

It is to be noted that this measurement for the conditions of perpendicular microwave and applied electric field vectors has been performed for the first time. Consideration of the results shows that it would be worthwhile also to take measurements on the variation of conductivity with applied electric field at varying angles between microwave and electric field vectors.

The variations of attenuation and phase shift constants of the semiconductor for the conditions of parallel and perpendicular microwave and applied electric field vectors are shown in Figure 13. For a completely filled guide, the attenuation and phase constants of the semiconductor decrease with applied electric field.

CHAPTER VII

POSSIBLE APPLICATION OF HIGH FIELD EFFECT

7.1 INTRODUCTION

A possible application of the anisotropic conduction of germanium under condition of a high electric field is the hot electron microwave rotator proposed by Gunn[14, 16]. The theoretical performance of such a rotator, which depends on the difference between microwave conductivities $\sigma_{\parallel}$ and $\sigma_{\perp}$ of Ge with electric field, has been discussed by Staecker and Das[30] and Engineer and Nag[31] assuming linear polarisation.

A more general solution for the performance of such a rotator is presented in this chapter.

7.2 THEORY

Consider a plane polarised wave $R_e[E_o\ e^{-\gamma z}\ e^{j\omega t}]$ which propagates in the z direction from the plane $z = 0$ in a piece of semiconductor with a propagation constant $\gamma = \alpha + j\beta$.

Application of a large electric field along the x-axis, results in anisotropic propagation ($\gamma_x \neq \gamma_y$). Let the electric field vector make an angle θ to the x-axis as shown in the figure 14, and resolve the wave into two components.

$$E_x = \vec{a}_x\ R_e\ [E_o\ \cos\theta\ e^{-\gamma_x z}\ e^{j\omega t}] \qquad (7.1)$$

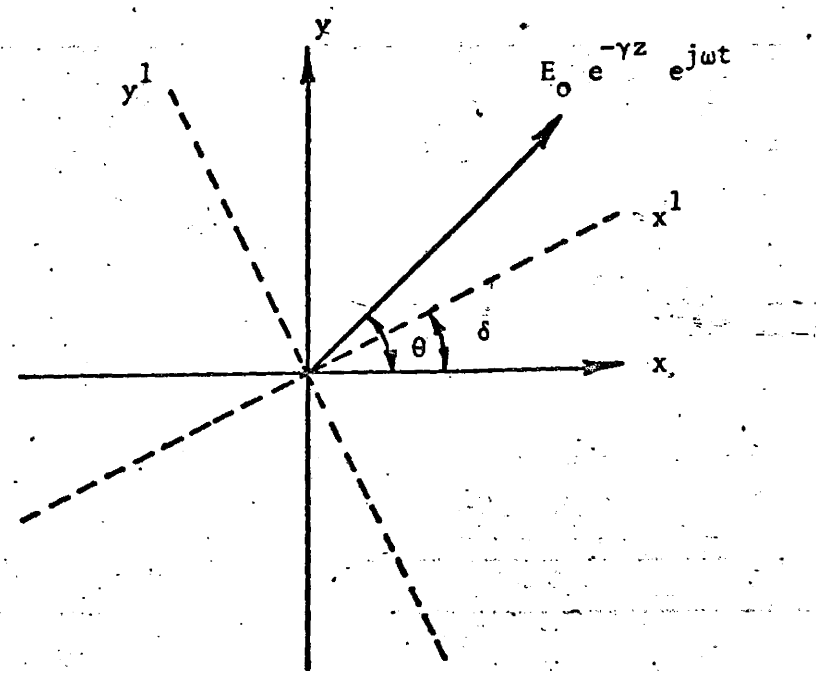

FIGURE 14: Plane Polarized wave
Propagating in Germanium

$$E_y = \vec{a}_y \, R_e \, [E_o \sin\theta \, e^{-\gamma_y z} \, e^{j\omega t}] \qquad (7.2)$$

Maxwell's curl equations for a T E M wave ($E_z = 0$, $H_z = 0$) in such an anisotropic propagating medium can be written as

$$\nabla \times \vec{H} = \vec{a}_x(\sigma_x + j\omega\varepsilon_x) \, E_x + \vec{a}_y \, (\sigma_y + j\omega\varepsilon_y) E_y \qquad (7.3)$$

$$\nabla \times \vec{E} = -j\omega\mu_o \, [\vec{a}_x \, H_x + \vec{a}_y \, H_y] \qquad (7.4)$$

The ℓ. h. s. of equations (7.3) and (7.4) can be expanded on the assumption of no variation with respect to x and y. Noting that

$$H_y \propto e^{-\gamma_x z} \qquad \frac{\partial H_y}{\partial z} = -\gamma_x \, H_y$$

$$H_x \propto e^{-\gamma_y z} \qquad \frac{\partial H_x}{\partial z} = -\gamma_y \, H_x$$

and by equations (7.1) and (7.2),

$$\frac{\partial E_x}{\partial z} = -\gamma_x \, E_x$$

$$\frac{\partial E_y}{\partial z} = -\gamma_y \, E_y \quad ,$$

equations (7.3) and (7.4) reduce to

$$\vec{a}_x \, \gamma_x \, H_y - \vec{a}_y \, \gamma_y \, H_x = a_x(\sigma_x + j\omega\varepsilon_x) \, E_x$$

$$+ \vec{a}_y(\sigma_y + j\omega\varepsilon_y) \, E_y \qquad (7.5)$$

$$\vec{a}_x \gamma_y H_y - \vec{a}_y \gamma_x E_x = -j\omega\mu_o [\vec{a}_x H_x + \vec{a}_y H_y] \qquad (7.6)$$

Equating the x components of (7.5) and the y components of (7.6)

$$\gamma_x = (\sigma_x + j\omega\epsilon_x) \frac{E_x}{H_y}$$

$$\gamma_x = j\omega\mu_o \frac{H_y}{E_x}$$

when $$\gamma_x = [-\omega^2 \epsilon_x \mu_o + j\omega\mu_o\sigma_x]^{1/2} \qquad (7.7)$$

and $$Z_x = \frac{E_x}{H_y}$$

$$= \frac{j\omega\mu_o}{\gamma_x}$$

$$= [\frac{j\omega\mu_o}{j\omega\epsilon_x + \sigma_x}]^{1/2}$$

$$= |Z_x| \, e^{j\phi_x} \qquad (7.8)$$

$$|Z_x| = [\frac{\omega\mu_o}{\sqrt{(\omega^2\epsilon_x^2 + \sigma_x^2)}}]^{1/2}$$

$$\phi_x = \frac{1}{2}[\frac{\pi}{2} - \tan^{-1} \frac{\omega\epsilon_x}{\sigma_x}]$$

Similarly, equating the y components of (7.5) and the x components of (7.6),

$$\gamma_y = [-\omega^2 \mu_o \varepsilon_y + j\omega\mu_o \sigma_y]^{1/2} \qquad (7.9)$$

$$Z_y = -\frac{E_y}{H_x}$$

$$= -\left(\frac{j\omega\mu_o}{\gamma_y}\right)$$

$$= \left[\frac{j\omega\mu_o}{j\omega\varepsilon_y + \sigma_y}\right]^{1/2}$$

$$= |Z_y|\, e^{j\phi_y} \qquad (7.10)$$

where $$|Z_y| = \left[\frac{\omega\mu_o}{\sqrt{(\omega^2 \varepsilon_y^2 + \sigma_y^2)}}\right]^{1/2}$$

and $$\phi_y = \frac{1}{2}\left[\frac{\pi}{2} - \tan^{-1}\frac{\omega\varepsilon_y}{\sigma_y}\right]$$

Writing the real parts of equation (7.1) and (7.2)

$$E_x = E_o \cos\theta\, e^{-\alpha_x z} \cos \omega_x t$$

$$E_y = E_o \sin\theta\, e^{-\alpha_y z} \cos \{\omega_x t - (\beta_y - \beta_x)z \qquad (7.11)$$

where $$\omega_x t = \omega t - \beta_x z$$

Eliminating 't' from equation (7.11), one can obtain,

$$\left[\frac{E_x}{E_o \cos\theta\ e^{-\alpha_x z}}\right]^2 + \left[\frac{E_y}{E_o \sin\theta\ e^{-\alpha_y z}}\right]^2 - 2\left[\frac{E_x}{E_o \cos\theta\ e^{-\alpha_x z}}\right]\left[\frac{E_y}{E_o \sin\theta\ e^{-\alpha_y z}}\right]$$

$$\cos(\beta_y-\beta_x)z = \sin^2(\beta_y-\beta_x)z \qquad (7.12)$$

which is the equation of an ellipse and shows that the wave become elliptically polarized as it progresses through the medium.

Equation (7.12) is not the standard form of the equation of an ellipse, because of the rectangular term $2\left[\frac{E_x}{E_o \cos\theta\ e^{-\alpha_x z}}\right]\left[\frac{E_y}{E_o \sin\theta\ e^{-\alpha_y z}}\right]\cos(\beta_y-\beta_x)z$ and can be converted to a simple form by rotation of the axes to the positions x^1-y^1 through an angle δ given by(32)

$$\tan 2\delta = \frac{-2(\cos\theta\ e^{-2\alpha_x z})(\sin\theta\ e^{-\alpha_y z})\cos(\beta_y-\beta_x)z}{\sin^2\theta\ e^{-2\alpha_y z} - \cos^2\theta\ e^{-2\alpha_x z}} \qquad (7.13)$$

The equation of the ellipse then becomes

$$\left[\frac{E_{x'}^2}{E_o^2 \sin^2(\beta_y-\beta_x)z}\right] \Big/ \left[\frac{\cos^2\delta}{\cos^2\theta\ e^{-2\alpha_x z}} - \frac{\cos(\beta_y-\beta_x)z \sin 2\delta}{\sin\theta\cos\theta\ e^{-\alpha_x z} e^{-\alpha_y z}} + \frac{\sin^2\delta}{\sin^2\theta\ e^{-2\alpha_y z}}\right] +$$

$$\left[\frac{E_y^2}{E_o^2 \sin^2(\beta_y-\beta_x)z \left[\frac{\sin^2\delta}{\cos^2\theta e^{-2\alpha_x z}} + \frac{\cos(\beta_y-\beta_x)z \sin 2\delta}{\sin\theta \cos\theta\, e^{-\alpha_x z} e^{-\alpha_y z}} + \frac{\cos^2\delta}{\sin^2\theta\, e^{-2\alpha_y z}}\right]}\right] = 1 \qquad (7.14)$$

or $$\frac{E_{x1}^2}{a^2} + \frac{E_{y1}^2}{b^2} = 1$$

where a = semi-major axis

= square root of the denominator of the first term in equation (7.14)

b = semi-minor axis

= square root of the denominator of the second term in equation (7.14)

and

$$\frac{a}{b} = \frac{\text{major axis}}{\text{minor axis}} \qquad (7.15)$$

The attenuation constants α_x, α_y and the phase constants β_x, β_y are obtained from equations (7.7) and (7.9).

It is, therefore, seen that the microwave field has not only been shifted by an angle

$$\psi = \theta - \delta \qquad (7.16)$$

but also rotates anticlockwise (for positive value of $(\beta_y-\beta_x)$) varying its magnitude with time.

It may be noted that linear polarization is a special case of elliptic polarisation when $\frac{a}{b} = \infty$ and for circular polarisation $\frac{a}{b} = 1$.

The average power carried by the wave is

$$P = \vec{a}_z \frac{1}{2} \text{Re} [E \times H^*]$$

$$= \vec{a}_z \frac{1}{2} \text{Re} \begin{vmatrix} a_x & a_y & a_z \\ E_x & E_y & o \\ H_x^* & H_y^* & o \end{vmatrix}$$

$$= \vec{a}_z \frac{1}{2} \text{Re} \left[E_x \left(\frac{E_x}{Z_x}\right)^* - E_y \left(-\frac{E_y}{Z_y}\right)^*\right]$$

$$= \vec{a}_z \frac{1}{2} \text{Re} \left[E_x \left(\frac{E_x e^{-j\phi_x}}{|Z_x|}\right)^* + E_y \left(\frac{E_y e^{-j\phi_y}}{|Z_y|}\right)^*\right] \text{[by equation (7.8) + (7.10)]}$$

Noting that $E = \vec{a}_x E_o \cos\theta \, e^{-\alpha_x z} e^{-j\beta_x z} + \vec{a}_y E_o \sin\theta \, e^{-\alpha_y z} e^{-j\beta_y z}$

with $e^{j\omega t}$ understood,

$$P = \vec{a}_z \frac{1}{2} \left[\frac{E_o^2 \cos^2\theta \, e^{-2\alpha_x z} \cos\phi_x}{|Z_x|} + \frac{E_o^2 \sin^2\theta \, e^{-2\alpha_y z} \cos\phi_y}{|Z_y|}\right]$$

and the power loss from the plane z = 0 is given by

$$P_{loss} = -10 \log_{10} \frac{P_z}{P_{z=0}}$$

$$= -10 \log_{10} \left[\frac{\cos^2\theta \, e^{-2\alpha_x z} \cos\phi_x |Z_y| + \sin^2\theta \, e^{-2\alpha_y z} \cos\phi_y |Z_x|}{\cos^2\theta \cos\phi_x |Z_y| + \sin^2\theta \cos\phi_y |Z_x|}\right] \quad (7.17)$$

The figure of merit F is defined as the ratio of angular shift to power loss, i.e.

$$F = \psi / \text{power loss (d.b.)} \qquad (7.18)$$

7.3 CALCULATIONS

Values of σ_x, σ_y at different values of electric fields were obtained from mobility vs. electric field curves using the results of Gunn[14], Gibson[12], Ryder[3] and Seeger[11]. These values then enabled exact solutions for $\gamma_x = \alpha_x + j\beta_x$ and $\gamma_y = \alpha_y + j\beta_y$ to be computed from equations (7.7) and (7.9).

Using the values of α_x, α_y and β_x, β_y thus obtained, calculations have been made of the angular shift, ratio of major and minor axis, the power loss and the figure of merit for different values of θ and z. The results are shown in figures 15 - 17.

7.4 DISCUSSION

Figure 15 gives the variation of power loss, angular shift and ratio of major and minor axes with z, using results of Gibson et al[12] for 4.68 ohm cm. n-Ge with T = 300°K, θ = 45° and the results of Seeger[11] for 21.5 ohm cm. n-Ge with T = 300°K, θ = 45°. It should be noted that for calculations shown as dashed lines, it has been assumed that σ_x is controlled by $\frac{\partial v}{\partial E}$ and approaches a negligible value at $f \lesssim 10$ GHz.

Figure 16 gives the variations of power loss, angular shift and figure of merit with θ and shows that the figure of merit is max. for

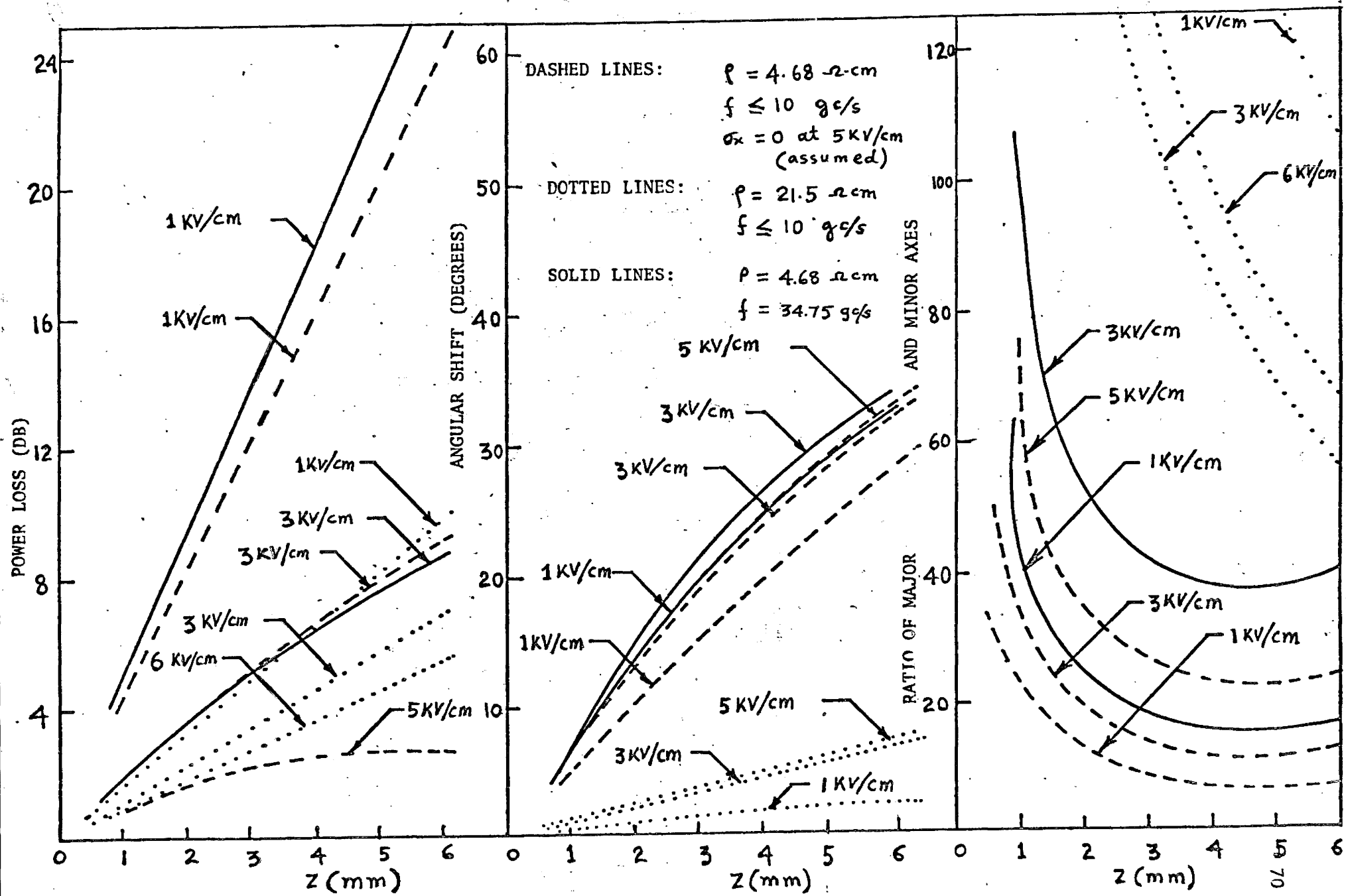

FIGURE 15: Variation of Power Loss, Angular Shift and Ratio of Major and Minor Axes with z

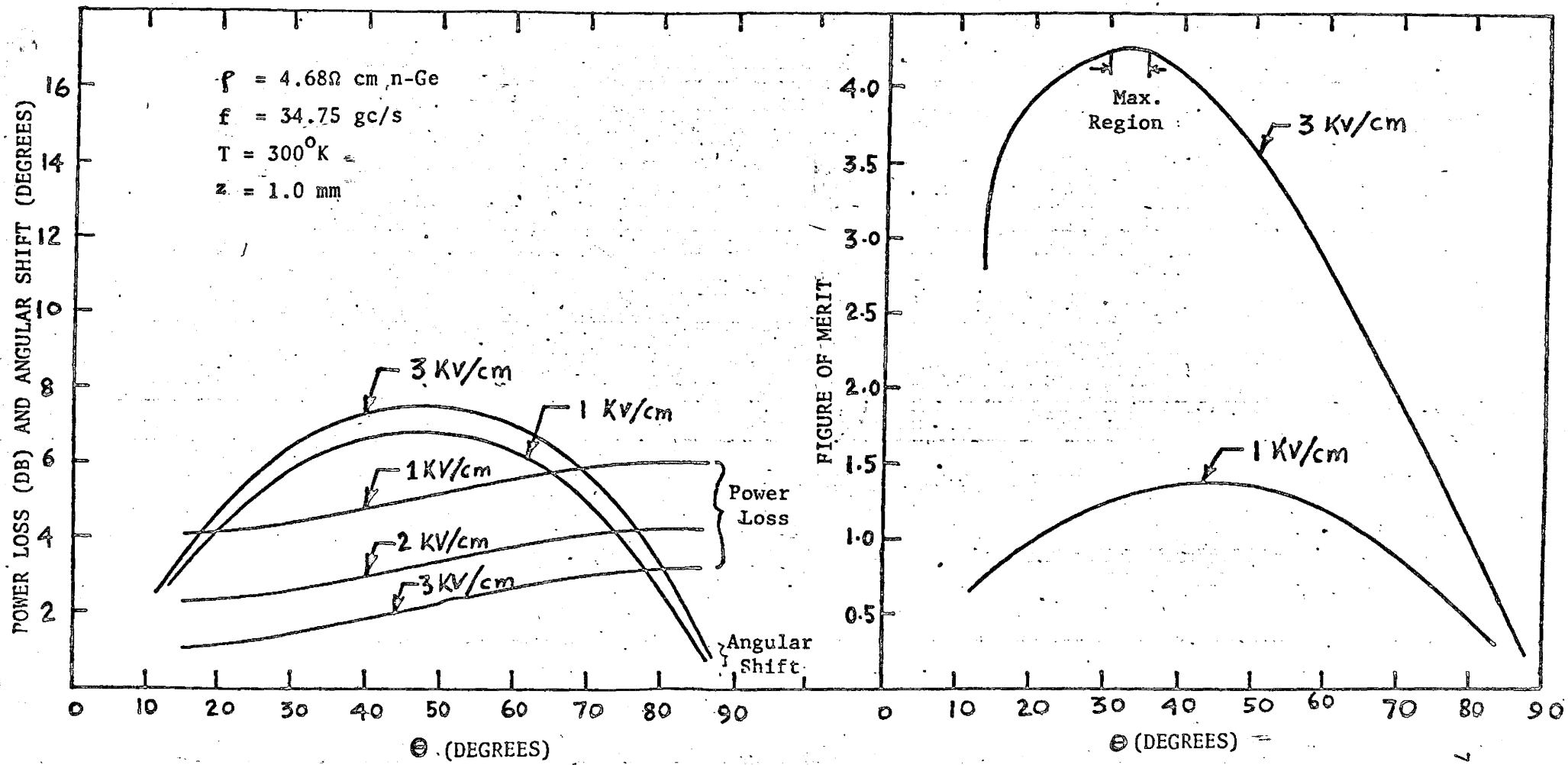

FIGURE 16: Variation of Power Loss, Angular Shift and Figure of Merit With θ

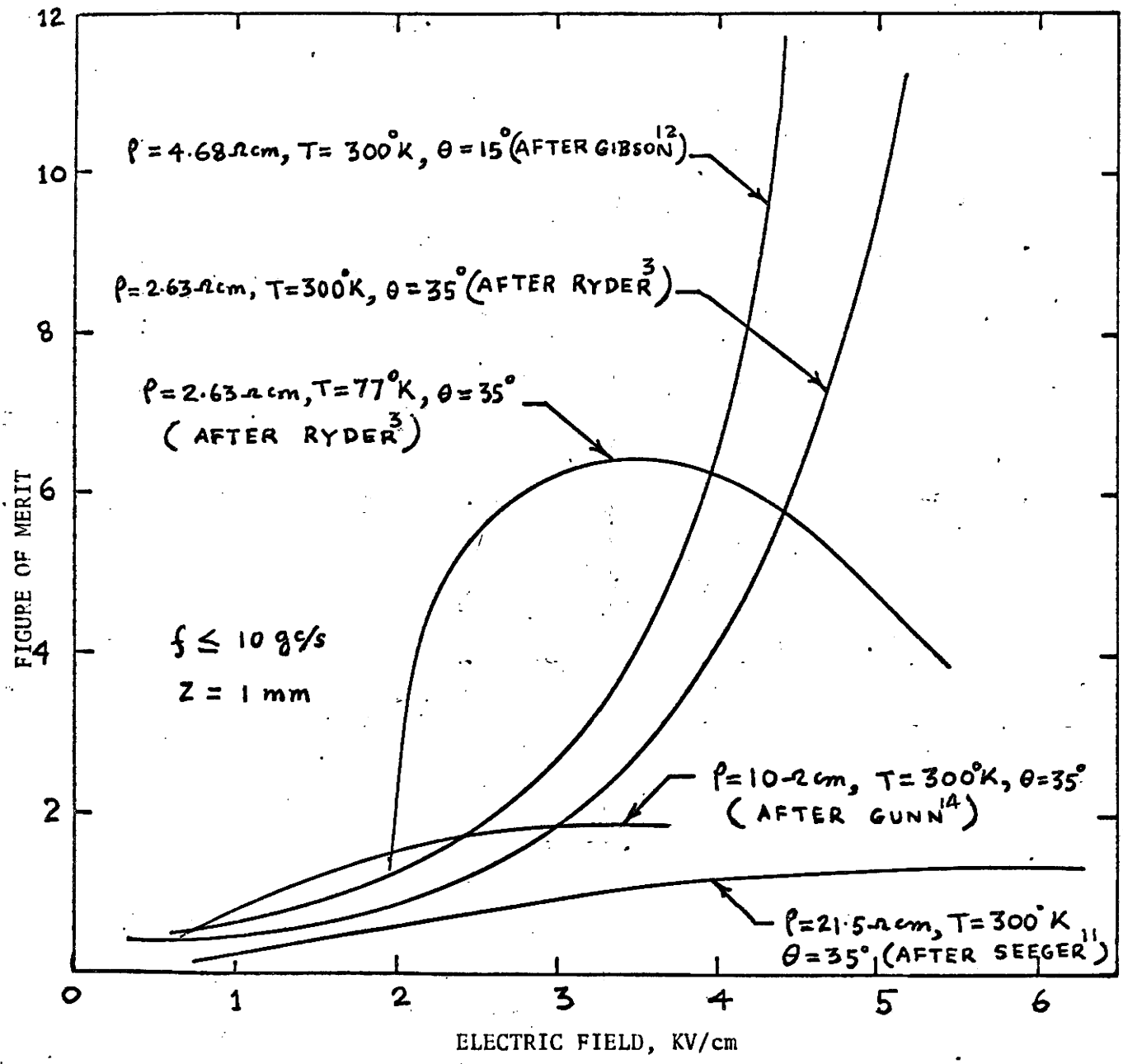

FIGURE 17: Dependence of Figure of Merit on Electric Field, Resistivity and Temperature for N-Type Germanium

$\theta = 30 - 35°$. Figure 17 shows the dependence of the figure of merit on electric field, resitivity and temperature.

CHAPTER VIII

CONCLUSIONS

1.

D. C. measurements have been made of the electron drift velocity in 10 ohm-cm. n-type germanium as a function of electric fields in the range 0 - 3KV/cm. These measurements, which are summarized in Figure 11, have been used for the determination of the d.c. mobility $\frac{v}{E}$ and the differential mobility $\frac{\partial v}{\partial E}$. These results are given in Figure 12 and provide a basis for comparison with the microwave measurements on the semiconductor which are described in this thesis.

2.

A new method for the measurement of the conductivity of a semiconductor subjected to a high electric (pulsed) field is described. The method utilizes a sensitive microwave reflection bridge (Figure 8) and measurements on 10 ohm-cm. n-type germanium subjected to fields 0 - 3KV/cm. have been carried out at 9.522 GHz. The klystron used as a signal source was capable of delivering high power (100 mw), which determined the sensitivity of the bridge. In the final form the bridge was capable of detecting attenuation change less than 0.1 db and phase changes of 0.01 mm (or 0.1°) in a semiconductor loaded wave guide

section, with an approximate loss of 5 db.

For the purposes of measurement, the semiconductor sample is placed at the end of a wave guide terminated by a short circuit, as shown in Figure 4. The input impedance at the air sample interface Z(o) is then obtained from the measurement of reflection co-efficient $\rho(o)$ with a microwave reflection bridge. The measured value of Z(o) is then used to calculate the propagation constant of microwaves propagating in the semiconductor as described in section 3.3. Knowledge of the value of the propagation constant then allows the calculation of the resistivity and dielectric constant of the semiconductor.

Theoretical expressions for the reflection co-efficient at a particular measuring plane in an ideal matched reflection bridge and also in a general bridge circuit are derived in section 3.2.

3.

Measurements have been made of the resistivity and dielectric constant of the 10 ohm-cm. germanium at 9.522 GHz, with the semiconductor sample inserted into a rectangular wave guide. The results are given in Table 5.2 and the value obtained for the resistivity is in good agreement with that measured by a d.c. 4 probe method. The probe measurements are given in Table 5.5.

4.

The conductivity of the sample was also measured at 9.522 GHz with varying electric fields with the results given in Table 5.3 and 5.4.

The microwave conductivity for the conditions of parallel microwave and applied electric field vectors gave a normalized carrier mobility, which agreed well with the values of differential mobility ($\frac{\partial v}{\partial E}$) obtained graphically from Figure 11. These results are in good agreement with those of Gunn[14] who performed measurements by a transmission bridge at a frequency of 9.392 GHz.

The mobility derived for the conditions of perpendicular microwave and applied electric field vectors is intermediate between $\frac{\partial v}{\partial E}$ and $\frac{v}{E}$ derived from drift velocity measurements. Measurements of the mobility applicable to the perpendicular field configuration have not been reported in the literature up to the present time.

For future investigation, it is recommended that measurements should be made to examine the variation of conductivity with electric field at varying angle between microwave and applied electric field vectors.

5.

The theoretical expressions for the propagation constant, the angular shift, the ratio of major and minor axes, power loss and figure of merit of a proposed hot electron microwave rotator, are developed.

It is seen that the plane of polarization of an electromagnetic wave in a semiconductor subjected to a high electric field is rotated by an angle. It is also seen that the wave becomes elliptically polarized as it progresses through the semiconductor and the microwave

field vector rotates anticlockwise [because of the positive value of $(\beta_y - \beta_x)$] varying its magnitude with time.

For a high figure of merit, it is desirable to use highly doped samples (2 - 5 ohm-cm.) or to operate at low temperature and to use a frequency <10 GHz with $30° < \theta < 35°$ (see Figure 17). However, for this condition the sample length is limited to 1 - 2 mm. For large angular shifts, it is necessary to increase the sample length, with a consequent increase in power loss (see Figure 15).

It may be noted that the characteristic to be sought for efficient rotator are small α_x and large $(\alpha_y - \alpha_x)$.

APPENDIX - I

COMPUTER PROGRAMMES

```
$JOB    WATFOR  093510 RAHMAN
$IBJOB          NODECK
$IBFTC
C       CALCULATION OF CS AND ZETA
      1 READ(5,2)ATTEN,PHASE,AO,ALO,AL,T
      2 FORMAT(6F10.5)
        A=.231*(ATTEN-AO)
        PHAI=2.9*(PHASE-ALO+AL)
        B=COSH(A)
        C=COS(PHAI)
        Z=SQRT((B-C)/(B+C))
        CS=Z/(1.45*T)
        ZETA=90.-(ATAN(SIN(PHAI)/SINH(A)))*57.29
        WRITE(6,3)CS,ZETA
      3 FORMAT(1H0,2F10.5)
        GO TO 1
      4 STOP
        END
$ENTRY
    2.10        1.705       0.0         1.583       0.0         0.157
    1.82        1.813       0.0         1.684       0.0         0.157
$IBSYS

                                        CD TOT    0022
```

```
$JOB    WATFOR  003510 RAHMAN
$IBJOB          NODECK
$IBFTC
C       CALCULATION OF RESISTIVITY AND DIELECTRIC CONSTANT
      1 READ(5,2)T,TAO,AL
      2 FORMAT(3F10.5)
        D=57.29
        A=COS(TAO/D)
        B=SIN(TAO/D)
        C=T/AL
        ALPHA=C*A
        BETA=C*B
        RO=375./(ALPHA*BETA)
        EPSI=(BETA*BETA-ALPHA*ALPHA-2.71)/8.99+1.0
        WRITE(6,3)ALPHA,BETA,RO,EPSI
      3 FORMAT(1H0,4F10.5)
        GO TO 1
      4 STOP
        END
$ENTRY
    1.5       69.7        0.157
    1.45      67.5        0.157
$IBSYS
```

CD TOT 0023

```
$JOB              03510 RAHMAN
C       SOLUTION OF PROPAGATION CONSTANT IN HOT ELECTRON PLASMA
        COMPLEX GAMMA,A,B,CMPLX,CSQRT
        WRITE(6,7)
    7   FORMAT(6X,4HVOLT,8X,7HEPSILON,1X,9HFREQUENCY,
       15X,5HSIGMA,5X,5HALPHA,6X,4HBETA)
    1   READ(5,2)VOLT,EPSI,F,SIGMA
    2   FORMAT(2F10.0,E10.3,F10.0)
        P=3.14159
        Y=2.*P*F*CSQRT(EPSI)*(P*34.416E-10)**0.5
        Z=SIGMA/(2.*P*F*EPSI*8.85E-12)
        A=CMPLX(0.,Y)
        B=CMPLX(1.,-Z)
        GAMMA=A*CSQRT(B)
        WRITE(6,3)VOLT,EPSI,F,SIGMA,GAMMA
    3   FORMAT(1H ,2F10.3,E10.3,F10.3,2E20.4)
        GO TO 1
    4   STOP                    /
        END
1000.0      16.0          9.392E098.2
1000.0      16.0          9.392E096.25
$IBSYS

                                  CD TOT    0022
```

```
$JOB            003510 RAHMAN
$IBJOB          NODECK
$IBFTC
C       GENERALISED SOLUTION OF MICROWAVE ROTATOR
        COMPLEX EMAJ,CMPLX
        WRITE(6,3)
    3 FORMAT(10X,1HZ,6X,6HALPHAX,1X,5HTHETA,3X,2HSI,
     13X,5HPHAIA,3X,5HPHAIB,3X,5HEMAJA,
     23X,5HEMINA,3X,5HEMAJB,3X,5HEMINB,2X,6HRATIOA,
     32X,6HRATIOB,3X,5HPLOSS,3X,5HAMERA,3X,5HAMERB)
    1 READ(5,2)ALPHAY,ALPHAX,BETAY,BETAX,FREQ,
     1EPSIY,EPSIX,EPSI,SIGMAY,SIGMAX,SIGMA
    2 FORMAT(4E10.4/4E10.4,3F5.2)
      THETA=15.0
    9 Z=0.001
      R=57.29
      W=THETA/R
      U=TAN(W)
    8 EX=EXP(-(ALPHAY-ALPHAX)*Z)
      EXPX=EXP(-ALPHAX*Z)
      EXPY=EXP(-ALPHAY*Z)
      V=(BETAY-BETAX)*Z
      C=COS(W)
      S=SIN(W)
      SI=.5*ATAN((U**2)*(EX**2)*SIN(2.0*V)/
     1(1.0+(U**2)*(EX**2)*COS(2.0*V)))
      T=V-SI
      D=ATAN(U*EX*COS(T)/COS(SI))*R
      PHAIA=THETA-D
      DELTA=.5*ATAN((-2.0*S*C*EXPX*EXPY*COS(V))/
     1(S**2*(EXPY**2)-C**2*(EXPX**2)))
      DELTAD=DELTA*R
      PHAIB=THETA-DELTAD
      PX=.5*(90./R-ATAN(6.28*FREQ*EPSIX/SIGMAX))
      PY=.5*(90./R-ATAN(6.28*FREQ*EPSIY/SIGMAY))
      PL=FREQ*6.28*1256.E-09
      PLX=SQRT(SIGMAX*SIGMAX+(FREQ*6.28)**2*(EPSIX*EPSIX))
      PLY=SQRT(SIGMAY*SIGMAY+(FREQ*6.28)**2*(EPSIY*EPSIY))
      PLIX=PL/PLX
      PLIY=PL/PLY
      PLXS=SQRT(PLIX)
      PLYS=SQRT(PLIY)
      PLOX=C**2*COS(PX)*PLYS
      PLOY=S**2*COS(PY)*PLXS
```

```
      PLU=PLUX*(EXPX)**2+PLUY*(EXPY)**2
      PLD=PLUX+PLUY
      PLOSS=-10.0*ALOG10(PLU/PLD)
      A=C*EXPX*COS(GI)
      B=S*EXPY*COS(T)
      Y=S*EXPY*SIN(T)
      EMAJ=CMPLX(A,B)
      EMAJA=ABS(EMAJ)
      EMINA=Y*COS(D/R)
      RATIOA=EMAJA/EMINA
      G=COS(V)*SIN(2.0*DELTA)/(S*C*EXPX*EXPY)
      E=(SIN(DELTA))**2/(C**2*(EXPX**2))+G+
     1(COS(DELTA))**2/(S**2*(EXPY**2))
      F=(COS(DELTA))**2/(C**2*(EXPX**2))-G+
     1(SIN(DELTA))**2/(S**2*(EXPY**2))
      EMAJB=SIN(V)/SQRT(F)
      EMINB=SIN(V)/SQRT(E)
      RATIOB=EMAJB/EMINB
      AMERA=PHAIA/PLOSS
      AMERB=PHAIB/PLOSS
      WRITE(6,7)Z,ALPHAX,THETA,SI,PHAIA,PHAIB,EMAJA,EMINA,
     1EMAJB,EMINB,RATIOA,RATIOB,PLOSS,AMERA,AMERB
    7 FORMAT(1H0,F10.3,E12.4,F6.1,F10.5,2F8.4,4F8.5,5F8.2)
      IF(Z.GT.0.005) GO TO 10
      Z=Z+.001
      GO TO 8
   10 IF(THETA.GT.80.0)GO TO 1
      THETA=THETA+10.0
      GO TO 9
    4 STOP
      END
$ENTRY
0.2661E 030.1640E 030.8398E 030.8132E 03
0.9390E 100.1685E-090.1685E-090.1685E-09 6.20 3.7010.00
$IBSYS

                                CD TOT   0035
```

APPENDIX - II

PHOTOGRAPHS

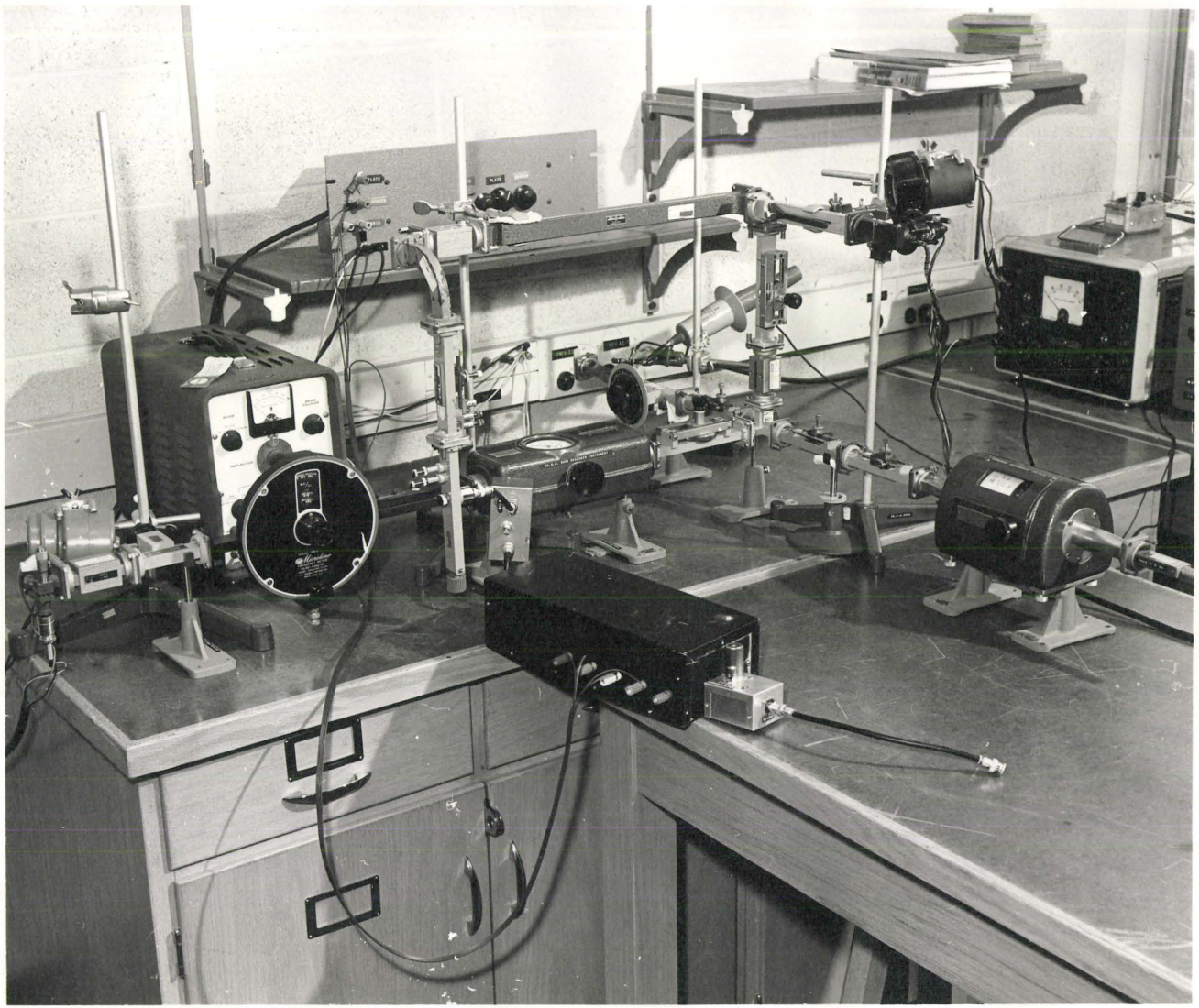

PHOTOGRAPH 1: The Experimental Setup of a Microwave Reflection Bridge for the Measurement of Propagation Constant in a 10Ω cm n-type Ge subjected to a High Electric Field.

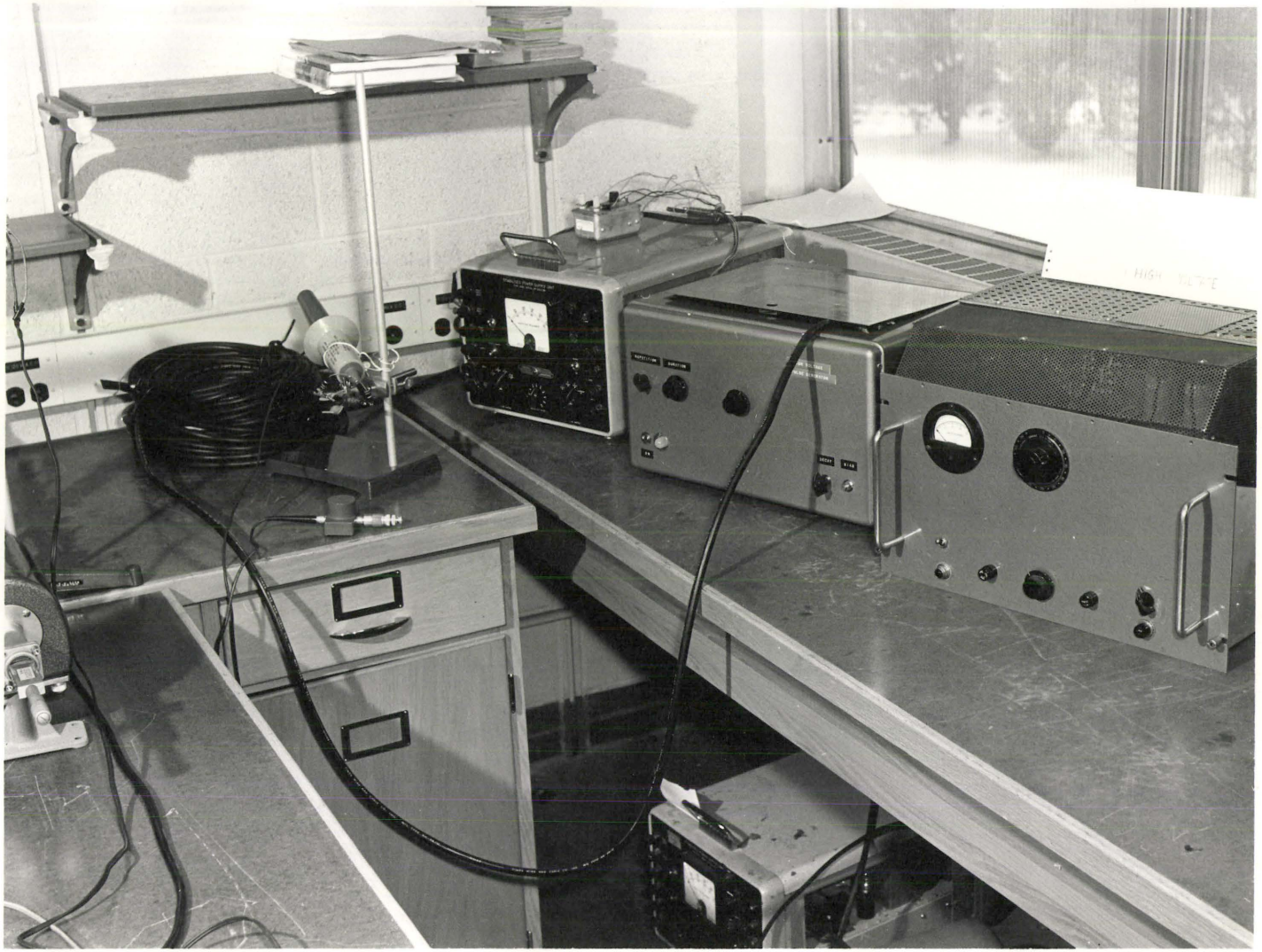

PHOTOGRAPH 2: The Pulse Generator, the Power Supply to the Pulse Generator and the High Voltage Supply.

REFERENCES

1. Fröhlich, H., "On the Theory of Dielectric Breakdown in Solids", Proc. Royal Soc. (London) A188, p. 521 (1947).

2. Ryder, E. J. and Shockley, W., "Mobilities of Electrons in High Electric Fields", Phy. Rev., Vol. 81, p. 139 (1951).

3. Ryder, E. J., "Mobility of Holes and Electrons in High Electric Fields", Phys. Rev., Vol. 90, p. 766 (1953).

4. Shockley, W., "Hot Electrons in Germanium and Ohm's Law", Bell Syst. Tech. J., Vol. 30, p. 990 (1951).

5. Gunn, J. B., "The Field Dependence of Electron Mobility in Germanium", Journal of Electronics, Vol. 2, p. 87 (1956).

6. Larrabee, R. D., "Drift Velocity Saturation in p-Type Germanium", J. Appl. Phys., Vol. 30, p. 857 (1959).

7. Gibbons, I. F., "Papers on Carrier Drift Velocities in Silicon at High Electric Fields", I. E. E. E. Transactions on Electric Devices", Vol. ED-14, No. 1, p. 37, (1967).

8. Gibson, A. F., "The Absorption of 39 GHz Radiation on Ge", Proc. Phys. Soc., London, B.69, p. 488 (1956).

9. Gibson, A. F. and Granville, J. W., "The Measurement of Drift Mobility in Germanium at High Electric Fields", J. Electronics, Vol. 2, p. 259 (1956).

10. Arthur, J. B., Gibson, A. F. and Granville, J. W., "The Effect of High Electric Fields on the Absorption of Germanium at Microwave Frequencies", J. Electronics, Vol. 2, p. 145 (1956).

11. Seeger, K., "Microwave Field Dependence of Drift Mobility in Germanium", Phys. Rev., Vol. 114, p. 476 (1959).

12. Gibson, A. F., Granville, J. W. and Paige, E. G., "A Study of Energy Loss Processes in Germanium at High Electric Fields Using Microwave Frequencies", J. Phys. Chem. Solids, Vol. 19, p. 198 (1961).

13. Nag, B. R. and Das, P., "Microwave Conductivity of Semiconductors in the Presence of High Steady Electric Fields", Phys. Rev., Vol. 132, p. 2514 (1963).

14. Gunn, M. W., "Hot Electron Effects in n-type Germanium at 9.392 GC/S", J. of Elect. Control., Vol. 16, p. 481 (1964).

15. Dykman, I. M. and Tolpygo, E. I., "Microwave Conductivity of Semiconductors with Carriers Heated by D. C. Field", Soviet Physics - Solid State, Vol. 7, p. 332 (1966).

16. Gunn, M. W., "The Microwave Conductivity of Germanium", Proc. I. E. E. E., Vol. 52, p. 851 (1964).

17. Shockley, W., "Electrons and Holes in Semiconductors", D. Van Nostrand Co., N. Y., (1951).

18. Moll, J. L., "Physics of Semiconductors", McGraw Hill, N. Y. (1964), p. 66, p. 206.

19. Smith, R. A., "Semiconductors", Cambridge (1959), p. 162.

20. Champlin, K. S. et al, "Explicit Forms for Conductivity and Permittivity of Bulk Semiconductors in Wave Guides", Proc. I. R. E., vol. 50. p. 232 (1961)

21. Champlin, K. S. et al, Dept. of Elect. Engg., University of Minesota, Minesota.

22. Roberts, S. and Von Hippel, A., "A New Method for Measuring Dielectric Constant and Loss in the Range of Centimeter Waves", J. Applied Phys., Vol 17, p. 610 (1946).

23. Sheikh, R. H., "The Microwave Measurement of Semiconductor Permittivity", M. Sc. Thesis, McMaster University, 1965, p. 43.

24. Waltz, M. C., "Electrical Contacts for Transistors and Diodes", Bell Lab. Records, p. 260, July (1955).

25. Dale, J. R. and Turner, R. G., "Simple Ohmic Contacts on Gallium Arsenide", Solid State Electronics, Vol. 6, p. 388, (1963).

26. Chan, T. M. Y., "The Microwave Measurement of the Conductivity of a Semiconductor Film", M. Eng. Thesis, McMaster University (1964).

27. Gunn, M. W., "A High Voltage Pulse Generator", Electronic Engg., Pg., 824, (1962).

28. Valdes, L. B., "Resistivity Measurements on Ge for Transistors", Proc. I. R. E., Vol. 42, p. 420 (1954).

29. Hunter, L. P., "Hand Book of Semiconductor Electronics", McGraw Hill, N. Y. 1962, p. 20-4.

30. Staecker, P. W. and Das, P., "Hot Electron Microwave Rotator", Proc. I. E. E. E., Vol. 52, p. 1766 (1965).

31. Engineer, M. H. and Nag, B. R., "On a Semiconductor Microwave Rotator Using Hot Carrier Properties", Proc. I. E. E. E., Vol. p. 429 (1966).

32. Durrant, J. E. and Kinston, H. R. "A New Analytic Geometry", The McMillan Company of Canada Ltd., 1944, p. 285.